

Lower-Hybrid Drift Instabilities in a magnetic nozzle

Matteo Ripoli,^{*} Eduardo Ahedo,[†] and Mario Merino[‡]

Department of Aerospace Engineering, Universidad Carlos III de Madrid, Leganés, Spain

(Dated: December 16, 2024)

Magnetic nozzles are a key component of electrodeless plasma thrusters, acting as their main acceleration stage. Non-stationary phenomena common to the entire range of $E \times B$ devices, such as oscillations and instabilities, are likely to exist in the magnetic nozzle, according to the mounting experimental evidence. These mechanisms could lead to anomalous cross-field transport, either enhancing the plasma plume divergence or favoring electron detachment. In this work we present a local linear analysis of fluid instabilities relevant for said devices, expanding on previous works with the addition of plasma inhomogeneities in the direction parallel to the magnetic field, with a rigorous inclusion of the effects of magnetic curvature, finite Larmor radius and 3D wave propagation, allowing for a general formulation of drift-driven instabilities in partially magnetized plasmas. Instability conditions are first studied analytically, and then applied to simulation data of a helicon plasma thruster. Finally, the effect of instabilities on wave-driven cross-field electron transport is assessed by means of quasi-linear analysis. This study predicts the onset of essentially-azimuthal instabilities in the 1 kHz–1 MHz range, in qualitative agreement with some of the available experimental data, and highlights the importance of including parallel inhomogeneities in the formulation of the dispersion relation of an $E \times B$ plasma, as these gradients may drive instabilities even in the absence of axial propagation. Lastly, quasi-linear analysis suggests that the induced cross-field transport acts to smooth out the zeroth-order drifts which cause the plasma to destabilize in the first place.

I. INTRODUCTION

A variety of plasma thrusters operate as partially magnetized $E \times B$ discharges, with electrons closely following magnetic field lines and the heavier ions moving almost freely from magnetic forces effects. Two notable classes of plasma thrusters are the Hall Thruster (HTs) [1–3] and Electrodeless Plasma Thrusters (EPTs)[4, 5] that rely on a magnetic nozzle (MN) [6] as their accelerating stage. $E \times B$ discharges are known to be subject to oscillations, instabilities, and turbulence [7], which under certain circumstances lead to non-classical transport of electrons across magnetic field lines, suggesting the existence of additional mechanisms not captured by usual steady-state electron models.

There is ample literature on the study of oscillations through local linear analysis, all sharing the common intention of finding sound physical principles and criteria behind onset of instability-driven anomalous transport in plasmas through a limited but analytically accessible formulation [8–13]. The assumption of locality is satisfied as long as the wavelength of the considered waves is considerably smaller than the shortest local characteristic length at equilibrium. For a two-species Maxwellian plasma at equilibrium, consisting of unmagnetized ions and magnetized electrons, the choice of studying its oscillations by means of either a fluid or a kinetic approach ultimately falls upon the scale of the considered problem. The fluid approach is generally considered valid as long as the perpendicular wavenumber times the equilibrium electron Larmor radius ρ_{e0} is a small number less than 1; in the parallel direction, the condition $|k_{\parallel} c_{e0}| < |\omega_e|$ needs to be respected, with k_{\parallel} , c_{e0} and ω_e the parallel wavenumber, the equilibrium

thermal electron velocity, and the wave frequency in the electron reference frame. This second condition implies that particles moving at a thermal velocity parallel to the magnetic field must be slower than the wave; at the same time, kinetic particle-wave interactions such as Landau damping are neglected. The advantages of employing a fluid approach over a kinetic one lie in its reduced complexity [14], at the price of assuming *a priori* the aforementioned upper limits on the perpendicular and parallel components of the wave vector \mathbf{k} .

HT plasmas have been thoroughly studied analytically, numerically and experimentally [7, 13, 15–18]. Oscillations have been found from the kHz to the tens of MHz ranges. Morozov et al. [19] employed a two-species fluid model with cold, inertialess electrons to justify experimentally observed azimuthally rotating structures. That work is one of the first to study the effect of plasma gradients and relative drift between plasma species on the onset of plasma instabilities, which will be referred to as *drift-gradient instabilities*. It was later expanded on by Esipchuk and Tulinin [20] with electron inertia and electromagnetic effects, by Frias et al. [21] with inertialess electrons with the addition of density and temperature gradients, by Escobar and Ahedo [22] with the inclusion of neutral dynamics and ionization collisions, and by Smolyakov et al. [23] with the inclusion of electron inertia and off-diagonal parts of the electron stress tensor, all of them sharing the common focus on HT plasmas. These last two works included the effect of *drift-resistive instabilities* as well, originating from the combination of relative inter-species drift and collisional effects, previously studied by Litvak and Fisch [24] for both electrostatic and electromagnetic waves. Ramos, Bello and Ahedo [11] provided a more general derivation of fluid electrostatic instabilities in $E \times B$ plasmas, examining in detail drift-gradient and drift-resistive instabilities in a variety of frequency and wavelength regimes along with *stream instabilities*, a class of unstable phenomena uniquely driven by relative drift between species, first presented by Bunemann [25].

^{*} PhD Student, mripoli@ing.uc3m.es

[†] Full Professor, eahedo@ing.uc3m.es

[‡] Full Professor, mario.merino@uc3m.es

Another work relevant to linear stability analysis of fluid electrostatic waves in HTs but from a global perspective is that of Bello and Ahedo [26], where numerical results of zeroth and first-order fluid models are obtained. Among the main findings of the work, the effect of including temperature perturbations is found to be non-negligible, but only for frequencies in the MHz range and greater.

Among the few works including wave propagation both along and across magnetic field lines, the one of Krall [27] from 1971 stands out. In the context of general $E \times B$ discharges, his proposed kinetic model was able to recover in the negligible Larmor radius limit ($k\rho_{e0} \ll 1$) results known from fluid theory plus a stream instability driven by parallel propagation.

In contrast, in the case of MNs and EPTs, not much work has been carried out in the analysis of their unsteady behaviour yet. Recent experimental works have indicated the presence of both azimuthal oscillations extending up to the hundreds of kHz [28–30] and azimuthal-axial oscillations [31, 32]. Desjardins and Gilmore [33] observe mainly-azimuthal fluctuations in geometrically-comparable linear plasma devices, in the kHz range. Various candidate frameworks have been proposed to explain these phenomena, from the destabilization of electrostatic lower hybrid waves in the work of Hepner et al. [31] to the magnetosonic wave in the work of Takahashi et al. [28], the latter being electromagnetic in nature. In the work of Desjardins and Gilmore [33], the oscillations are identified as a mixture of drift-resistive electron drift waves and Kelvin-Helmoltz instabilities.

Moreover, the role of instabilities in MNs is not clear, and the literature presents clashing arguments on the effect and the direction of wave-driven transport. Hepner et al. [31] propose an outward electron flux, relaxing the density gradient and reducing the device efficiency, while Takahashi et al. [28] suggest an inward particle flux, pushing the plasma towards its axis of symmetry.

The naming conventions for instabilities in partially magnetized plasmas are abundant, and at times conflicting. Two main labelling categories can be identified, relevant to two different frequency regimes: the Electron Cyclotron Drift Instability (ECDI) [13, 18], relevant to frequencies comparable to harmonics of the electron gyrofrequency in the electron frame, and the Lower-Hybrid Drift Instabilities (LHDI) [23, 31, 34], relevant instead to frequencies close to the lower-hybrid frequency. Notable fluid limits of the latter are the drift-gradient Modified Simon-Hoh Instability (MSHI) [23] and the Modified Two-Stream Instability (MTSI) [27].

What stands out from the existing body of work on $E \times B$ discharges is that many of the identified instabilities are particular limits of a more general dispersion relation. In fact, it can be stated that a whole family of *fluid* instabilities stems from the presence of a non-zero interspecies drift, be it gradient-driven or otherwise, allowing the presence of ‘slow’ waves with phase velocity smaller than the drift velocity, or, in other terms, with negative Doppler-shifted frequency. These waves can be described as carrying negative energy [35]: when coupled with an energy sink—either a positive energy wave or a dissipative process such as inelastic collisions—they can be-

come unstable [36].

All of the above is based on a 1D description of equilibrium gradients, as it is the relevant case in HTs, Penning and magnetron discharges. In this work we derive a comprehensive formulation for electrostatic drift waves, taking into account inertial, gyroviscous, collisional and 2D gradient effects as well as 3D wave propagation, conditions relevant to MNs and EPTs. The combination of all the aforementioned contributions results in a dispersion relation from which novel instability criteria can be obtained, considerably more general than the ones present in the literature. Most noticeably, the inclusion of parallel gradients of equilibrium plasma quantities other than perpendicular ones allows for an easier destabilization of the plasma, given the difference in thermal velocities between the species. The derivation is carried out in a fluid framework, assuming cold, unmagnetized ions and warm electrons. We will assume long wavelengths, with the aforementioned limit on the perpendicular wavenumber and $|k_{\parallel}c_{e0}| < |\omega_e|$, and we will perform a cartesian expansion to study an axisymmetric problem. We further assume our plasma to have isotropic temperature at equilibrium and neglect temperature oscillations. Consequently in the following, for brevity, we drop the subscript 0 on equilibrium magnetic field and temperature and related magnitudes, so that $B \equiv B_0$, $T_e \equiv T_{e0}$, etcetera.

We focus on the low-to-mid frequency range $\omega_{ci} \ll \omega < \omega_{ce}$, with ω_{cs} being the equilibrium cyclotron for the s -th species ($i = \text{ions}$, $e = \text{electrons}$), and work with power expansions on the small parameter $\varepsilon = \rho_e/L \ll 1$, with L being the shortest local characteristic length at equilibrium. An *a priori* choice has to be made on the order of magnitude of the inertial terms with respect to the cyclotron terms, i.e. whether the electron Doppler-shifted frequency $\omega_e \equiv \omega - \mathbf{k} \cdot \mathbf{u}_{e0}$ is comparable with ω_{ce} or with $\omega_{ce} O(\rho_e/L)$. We will refer to the former choice as to the ‘High-Frequency’ (HF) regime, while to the latter as the ‘Low-Frequency’ (LF) one, a differentiation similar to that presented in [11]. The obtained dispersion relation is then applied to hybrid PIC/fluid/wave simulations of MNs from Jimenez et al. [37] as input for the equilibrium plasma quantities and gradients, in order to investigate the eventual triggering for instabilities in these devices. The predicted instabilities propagate predominantly in the azimuthal direction, with frequencies ranging between 1 kHz and 1 MHz. The presence of parallel gradients of equilibrium plasma quantities considerably widens the unstable regions of the discharge, allowing for the onset of exponential wave growth even when the conditions for ‘classical’ instabilities coming the literature (such as the MSHI and the MTSI) are not met. The findings are qualitatively contrasted with available experimental data.

The rest of the paper is structured as follows: in section II we will show the employed fluid model and the general derivation procedure of the dispersion relation in the LF regime. In section III we will obtain the detailed formulation of the dispersion relation, comparing it with formulations found in literature. In section IV we will show analytical solutions of the LF dispersion relation, expressing general instability criteria for both drift-gradient and drift-dissipative perturbations. In

section V we will specialize the dispersion relation to a simulated MN plasma using the data from Jimenez et al. [37] as input for the equilibrium plasma quantities and gradients. In section VI we will model the effect of unstable oscillations on cross-field fluxes and velocities through quasi-linear analysis. Finally, in section VII we will present a summary and discuss the main findings of this work. A preliminary version of this work has been presented as a conference paper in [38], where the iterative procedure needed to derive the HF dispersion relation was discussed as well.

II. FLUID MODEL

This section presents the derivation procedure of the local, linear, electrostatic dispersion relation for an $E \times B$ two-fluid plasma composed of cold, unmagnetized ions i , and warm, thermally isotropic, magnetized electrons e . The model retains perpendicular and parallel gradients, wave propagation in all three directions, gyroviscous tensor terms and collisional phenomena. The model is consistent up to the $O(\varepsilon)$ order.

Our main focus of application is an axisymmetric MN, with the axis of symmetry coinciding with the z axis, we define the local coordinate system $\{\mathbf{1}_{\parallel}, \mathbf{1}_{\perp}, \mathbf{1}_{\theta}\}$, with $\mathbf{1}_{\parallel} = \mathbf{B}/B$, $\mathbf{1}_{\theta}$ perpendicular to the (z, r) meridian plane, and $\mathbf{1}_{\perp} = \mathbf{1}_{\theta} \times \mathbf{1}_{\parallel}$. Due to the zeroth-order axisymmetry of the discharge, gradients of the zeroth-order quantities are contained in the $(\mathbf{1}_{\parallel}, \mathbf{1}_{\perp})$ plane.

For our analysis to be local we require the wavenumber to satisfy $kL = k\rho_e/\varepsilon \gg 1$. We will make use of a cartesian expansion to study an axisymmetric problem, neglecting cylindrical terms. Thus, the azimuthal wavenumber must respect $|rk_{\theta}| \gg 1$. Being our model fluid, we limit the normalized perpendicular wavenumber to values $k_{\perp}\rho_e < 1$, with $k_{\perp} = (k_{\perp}^2 + k_{\theta}^2)^{1/2}$, $\rho_e = c_e/\omega_{ce}$ the electron gyroradius at equilibrium, ω_{ce} the equilibrium electron gyrofrequency, $c_e^2 \equiv T_e/m_e$ the equilibrium electron thermal velocity and m_e the electron mass. For the same reason, in the parallel direction, where motion of electron particles is essentially the free thermal drift, the wavelength must be larger than the distance covered by a single particle during an oscillation, a condition which can be expressed as $|k_{\parallel}c_e| < |\omega_e|$.

A. General electron equations

Warm, magnetized electrons are described by their continuity and momentum equations, which read:

$$\frac{\partial n_e}{\partial t} + \nabla \cdot (n_e \mathbf{u}_e) = v_p n_e, \quad (\text{II.1})$$

$$\frac{\partial \mathbf{u}_e}{\partial t} + \mathbf{u}_e \cdot \nabla \mathbf{u}_e = -\frac{\nabla \cdot \bar{\bar{p}}_e}{m_e n_e} - \frac{e}{m_e} (-\nabla \phi + \mathbf{u}_e \times \mathbf{B}) - v_e \mathbf{u}_e, \quad (\text{II.2})$$

where v_p represents the particle production rate, ϕ the electrostatic potential, v_e is used to model dissipative forces on the electrons coming from collisional phenomena, and $\bar{\bar{p}}_e$ the

complete electron pressure tensor including the gyroviscous contribution. The system has to be completed with the energy equation, which we are not going to consider in the perturbation problem since we are neglecting temperature perturbations, i.e., $T_{e1} = 0$. This assumption is reasonable for low frequency oscillations [26].

Under the assumption of small amplitude waves, each quantity Q in the equations above is expanded as a zeroth-order, time independent part, plus a first-order contribution, through which we will model any oscillatory phenomena,

$$Q(\mathbf{x}, t) = Q_0(\mathbf{x}) + \frac{1}{2}[Q_1(\mathbf{x}) \exp(i\mathbf{k} \cdot \mathbf{x} - i\omega t) + CC], \quad (\text{II.3})$$

with $\mathbf{x} = s_{\perp} \mathbf{1}_{\perp} + s_{\theta} \mathbf{1}_{\theta} + s_{\parallel} \mathbf{1}_{\parallel}$, being $s_{\perp, \theta, \parallel}$ local coordinates about the point of analysis, and with the subscripts 0 and 1 referring to equilibrium values and their first-order corrections, respectively. The nomenclature CC serves as a reminder that complex conjugates need to be added to recover a real quantity; in the following it is omitted for brevity. Note that solutions with $\omega_r < 0$ are equivalent to solutions with $\omega_r > 0$ but opposite sign of the components of \mathbf{k} , with $\omega_r \equiv \text{Re}\{\omega\}$. It is easy to check that the first-order terms of the gradient of Q is composed of two contributions,

$$i\mathbf{k}Q_1 + \nabla Q_1, \quad (\text{II.4})$$

with $|\nabla \ln Q_1| = k O(\varepsilon)$ by assumption.

B. Zeroth-order equilibrium

In this work, the zeroth-order equilibrium plasma quantities and gradients are taken from the hybrid (PIC/fluid/wave) simulations of the MN of a helicon plasma thruster, presented in [37]. The full detail of the model, its numerical implementation, and the results can be found in that work and references therein. These simulations implement essentially the same electron equations as above, except that they drop electron inertia, temperature anisotropies and gyroviscous terms for the electron equilibrium in Eq. (II.2), consider a scalar electron pressure $\bar{\bar{p}}_{e0} = p_{e0}I$ with $p_{e0} = n_{e0}T_e$. They also implement an energy equation for the electron temperature T_e , together with a heat flux closure, which here is not considered as first-order perturbations will be considered isothermal. Ions and neutrals are treated kinetically as macroparticles. The collisional mechanisms considered are: single and double ionization; elastic electron-neutral and electron-ion collisions; neutral excitation collisions. These zeroth-order solutions are just used for a quantitative assessment of the first-order perturbation model.

C. First-order perturbation equations

We next model the first-order electrostatic (i.e. $B_1 = 0$) perturbations. For simplicity, the perturbation of the pressure tensor is modelled $\bar{\bar{p}}_{e1} = p_{e1}I + \Pi_{e1}$, with $p_{e1} = n_{e1}T_e$ and Π_{e1} is the perturbed gyroviscous tensor. The zeroth and first-order

terms of the divergence of Π_e , relevant in the following, are given in appendix A.

In linearized perturbed form, the continuity equation (II.1) for electrons reads

$$-i\omega n_{e1} + n_0 (\nabla \cdot \mathbf{u}_{e1} + \mathbf{u}_{e1} \cdot \nabla \ln n_0) + \mathbf{u}_{e0} \cdot \nabla n_{e1} + n_{e1} \nabla \cdot \mathbf{u}_{e0} = v_p n_{e1}. \quad (\text{II.5})$$

Defining the Doppler-shifted frequency as $\omega_e \equiv \omega - \mathbf{k} \cdot \mathbf{u}_{e0}$ and the normalized number density as $h_{e1} \equiv n_{e1}/n_{e0}$, and rearranging terms, this becomes

$$-i\omega_e h_{e1} + \mathbf{u}_{e0} \cdot \nabla h_{e1} + i\mathbf{k} \cdot \mathbf{u}_{e1} + \nabla_{\perp} u_{\perp e1} + \nabla_{\parallel} u_{\parallel e1} - u_{\perp e1} \nabla_{\perp} \ln B - u_{\parallel e1} \nabla_{\parallel} \ln B + \mathbf{u}_{e1} \cdot \nabla \ln n_0 = -h_{e1} \left(\frac{\nabla \cdot (n_0 \mathbf{u}_{e0})}{n_0} - v_p \right), \quad (\text{II.6})$$

with the directional derivatives $\nabla_{\perp} = \mathbf{1}_{\perp} \cdot \nabla$ and $\nabla_{\parallel} = \mathbf{1}_{\parallel} \cdot \nabla$. The first-order electron momentum equation (II.2), projected along $\mathbf{1}_{\perp}, \mathbf{1}_{\theta}, \mathbf{1}_{\parallel}$, yields, respectively,

$$u_{\perp e1} \left[-i\omega_e + v_e + \mathbf{u}_{e0} \cdot \nabla \ln u_{\perp e1} + \nabla_{\perp} u_{\perp e0} - (\nabla_{\parallel} \ln B) u_{\parallel e0} \right] + u_{\theta e1} \omega_{ce} + u_{\parallel e1} \left[\nabla_{\parallel} u_{\perp e0} - (\nabla_{\parallel} \ln B) u_{\perp e0} + 2(\nabla_{\perp} \ln B) u_{\parallel e0} \right] = -\frac{ik_{\perp} p_{e1} + \nabla_{\perp} p_{e1}}{m_e n_0} - \frac{(\nabla \cdot \Pi_{e1})_{\perp}}{m_e n_0} + \left(\frac{\nabla_{\perp} p_{e0}}{m_e n_0} + \frac{(\nabla \cdot \Pi_{e0})_{\perp}}{m_e n_0} \right) h_{e1} + (ik_{\perp} + \nabla_{\perp} \ln \phi_1) \frac{e\phi_1}{m_e}, \quad (\text{II.7})$$

$$u_{\perp e1} [-\omega_{ce} + \nabla_{\perp} u_{\theta e0}] + u_{\theta e1} [-i\omega_e + v_e + \mathbf{u}_{e0} \cdot \nabla \ln u_{\theta e1}] + u_{\parallel e1} \nabla_{\parallel} u_{\theta e0} = -\frac{ik_{\theta} p_{e1}}{m_e n_0} - \frac{(\nabla \cdot \Pi_{e1})_{\theta}}{m_e n_0} + \frac{(\nabla \cdot \Pi_{e0})_{\theta}}{m_e n_0} h_{e1} + ik_{\theta} \frac{e\phi_1}{m_e}, \quad (\text{II.8})$$

$$u_{\perp e1} [-2(\nabla_{\parallel} \ln B) u_{\perp e0} + \nabla_{\perp} u_{\parallel e0} - (\nabla_{\perp} \ln B) u_{\parallel e0}] + u_{\parallel e1} [-i\omega_e + v_e + \nabla_{\parallel} u_{\parallel e0} - (\nabla_{\perp} \ln B) u_{\perp e0}] + \mathbf{u}_{e0} \cdot \nabla u_{\parallel e1} = -\frac{ik_{\parallel} p_{e1} + \nabla_{\parallel} p_{e1}}{m_e n_0} - \frac{(\nabla \cdot \Pi_{e1})_{\parallel}}{m_e n_0} + \left(\frac{\nabla_{\parallel} p_{e0}}{m_e n_0} + \frac{(\nabla \cdot \Pi_{e0})_{\parallel}}{m_e n_0} \right) h_{e1} + (ik_{\parallel} + \nabla_{\parallel} \ln \phi_1) \frac{e\phi_1}{m_e}. \quad (\text{II.9})$$

Defining $\mathbf{Q}_e = [h_e, u_{\perp e}, u_{\theta e}, u_{\parallel e}]^T$, Eqs. (II.6) to (II.9) can be cast in matrix form as

$$\mathbf{Q}_{e1} = A_e^{-1} \mathbf{K} \frac{e\phi_1}{m_e}, \quad (\text{II.10})$$

where $\mathbf{K} = [0, ik_{\perp} + \nabla_{\perp} \ln \phi_1, ik_{\theta}, ik_{\parallel} + \nabla_{\parallel} \ln \phi_1]^T$ and the 4×4 matrix A_e depends on zeroth-order plasma quantities, their gradients and on the gradients of their first-order perturbations, symbolically written as $A_e = A_e(\omega_s, \mathbf{k}, \mathbf{Q}_{e0}, \nabla \mathbf{Q}_{e0}, \nabla \mathbf{Q}_{e1})$. It is important to note here that, for any Q_{e0} and Q_{e1} , $O(\rho_e \nabla \ln Q_{e0}) = O(\rho_e \nabla \ln Q_{e1}) = O(\varepsilon)$, thus requiring both of them to be retained in A_e at that order. Eq. (II.10) is implicit in $\nabla \mathbf{Q}_{e1}$: the recurrence can be resolved by assuming a weakly inhomogeneous plasma, ne-

glecting second order spatial derivatives of any Q_{e0} and Q_{e1} :

$$\frac{\partial \mathbf{Q}_{e1}}{\partial x_k}(\phi_1, \mathbf{k}, \mathbf{Q}_{e0}, \nabla \mathbf{Q}_{e0}, \nabla \mathbf{Q}_{e1}) \simeq \frac{\partial \mathbf{Q}_{e1}}{\partial \phi_1} \frac{\partial \phi_1}{\partial x_k} + \sum_{\substack{Q_{e0} \in \{n_0, \\ T_e, B, \mathbf{u}_{e0}\}}} \frac{\partial \mathbf{Q}_{e1}}{\partial Q_{e0}} \frac{\partial Q_{e0}}{\partial x_k}, \quad (\text{II.11})$$

so that $A_e \simeq A_e(\omega, \mathbf{k}, \mathbf{Q}_{e0}, \nabla \mathbf{Q}_{e0}, \nabla \ln \phi_1)$ and \mathbf{Q}_{e1} can be expressed as a function of ϕ_1 and $\nabla \ln \phi_1$ alone.

The zeroth-order electron drift velocity $u_{\theta e0}$ is one of the relevant parameters for the expansion. In equilibrium, $u_{\theta e0}$ results from the sum of an $E \times B$ drift and a diamagnetic drift. Only the Low-Frequency (LF) limiting cases will be analysed here, where $u_{\theta e0} = O(c_e \varepsilon)$ and $\omega_e = O(\omega_{ce} \varepsilon)$, relevant for LHDI. The equilibrium electron parallel velocity, on the other hand, will be assumed to be at most of the order of the ion sound speed, $|u_{\parallel e0}| \leq O(c_s)$, with $c_s^2 \equiv T_e/m_i$ the ion sound speed and m_i the ion mass.

D. Ion solution

Cold, unmagnetized, singly-charged ions are described by the same Eqs. (II.1) to (II.2), neglecting the magnetic force ($B = 0$), pressure tensor ($\bar{p}_i = 0$), and collisional momentum exchange ($v_i = 0$). Otherwise, the same procedure as above applies, mutatis mutandi (e.g. substituting e with i).

Ion motion at equilibrium is of order $u_{i0} \leq O(c_s)$, consistently with other studies and observations of MNs [39–41]. Keeping only $O(1)$ terms, the ion system yields

$$\frac{h_{i1}}{e\phi_1/m_i} = \frac{k^2}{\omega_i^2}, \quad (\text{II.12})$$

$$\frac{u_{i1}}{e\phi_1/m_i} = \frac{k}{\omega_i}. \quad (\text{II.13})$$

E. Poisson's equation

Once h_{i1} and h_{e1} have been found as functions of ϕ_1 , a closure relation for ϕ_1 is needed. One possibility is, naturally, to employ Poisson's equation. Neglecting second order spatial

derivatives:

$$\begin{aligned} \frac{n_0 e}{\epsilon_0} (h_{i1} - h_{e1}) = -\nabla^2 \phi_1 = & \\ \left[k^2 - (2ik_{\perp} - \nabla_{\perp} \ln B) \nabla_{\perp} \ln \phi_1 - (\nabla_{\perp} \ln \phi_1)^2 \right. & \\ \left. - (2ik_{\parallel} - \nabla_{\parallel} \ln B) \nabla_{\parallel} \ln \phi_1 - (\nabla_{\parallel} \ln \phi_1)^2 \right] \phi_1, & \quad (\text{II.14}) \end{aligned}$$

with ϵ_0 the vacuum dielectric permittivity. Alternatively, the system can be closed with the assumption of quasineutrality, which is just the $\epsilon_0 \rightarrow 0$ limit of Eq. (II.14), i.e. $h_{i1} = h_{e1}$. This is also the limit found for $\omega_{pi}^2 \gg \omega_i^2$ in Eq. (II.14), with $\omega_{ps}^2 = n_0 e^2 / (m_s \epsilon_0)$ ($s = i, e$) the plasma frequency of the s -th species, and hence we shall use this for the low frequency dispersion relation.

III. LOW FREQUENCY DISPERSION RELATION

In the LF case, ω_e and $u_{\theta e0}$ are of order $O(\epsilon)$ with respect to ω_{ce} and c_e respectively. Recalling the conditions for the validity our model, we impose the upper limits on the perpendicular wavenumber $k_{\perp} \rho_e < 1$ and on the parallel wavenumber $|k_{\parallel} c_e| < |\omega_e|$; this last condition, in the present case, implies $|k_{\parallel} \rho_e| \leq O(\epsilon)$.

With the chosen ordering for $u_{\theta e0}$, the inertial convective terms appear as $O(\epsilon^2)$ terms and are therefore neglected. In the following we will make use of the following definitions:

$$\omega_{\perp} \equiv \omega_e - \frac{k_{\theta} c_e^2}{2\omega_{ce}} \nabla_{\perp} \ln \left(\frac{p_{e0}}{B^2} \right), \quad (\text{III.1})$$

$$\omega_{\parallel} \equiv \omega_e - \frac{k_{\theta} c_e^2}{\omega_{ce}} \nabla_{\perp} \ln \left(\frac{p_{e0}}{B^4} \right), \quad (\text{III.2})$$

which are the Doppler-shifted frequencies multiplying the velocity in the directions perpendicular and parallel to the magnetic field respectively, accounting for gyroviscous cancellation[42]. Substituting the expression for the gyroviscous tensor from appendix A and keeping only $O(\epsilon)$ terms, the linearized electron system of Eqs. (II.6) to (II.9) becomes:

$$-i\omega_e h_{e1} + \left[ik_{\perp} + \nabla_{\perp} \ln \left(\frac{n_0 u_{\perp e1}}{B} \right) \right] u_{\perp e1} + ik_{\theta} u_{\theta e1} + \left[ik_{\parallel} + \nabla_{\parallel} \ln \left(\frac{n_0 u_{\parallel e1}}{B} \right) \right] u_{\parallel e1} = 0. \quad (\text{III.3})$$

$$\begin{aligned} c_e^2 \left[ik_{\perp} + \nabla_{\perp} \ln h_{e1} \right] h_{e1} - i \left[\omega_{\perp} + i v_e \right] u_{\perp e1} + \left[\omega_{ce} \left(1 - \frac{k^2 \rho_e^2}{2} \right) + i \frac{k_{\perp} c_e^2}{\omega_{ce}} \nabla_{\perp} \ln \left(\frac{\sqrt{p_{e0}} u_{\theta e1}}{B} \right) \right] u_{\theta e1} \\ + i \frac{k_{\theta} c_e^2}{\omega_{ce}} \left[ik_{\parallel} + \nabla_{\parallel} \ln \left(\frac{p_{e0} u_{\parallel e1}}{B^{5/2}} \right) \right] u_{\parallel e1} = \left[ik_{\perp} + \nabla_{\perp} \ln \phi_1 \right] \frac{e\phi_1}{m_e}, \quad (\text{III.4}) \end{aligned}$$

$$ic_e^2 k_\theta h_{e1} - \left[\omega_{ce} \left(1 - \frac{k^2 \rho_e^2}{2} \right) + i \frac{k_\perp c_e^2}{\omega_{ce}} \nabla_\perp \ln \left(\frac{\sqrt{P_{e0}} u_{\perp e1}}{B} \right) \right] u_{\perp e1} - i [\omega_\perp + i\nu_e] u_{\theta e1} - i \frac{k_\perp c_e^2}{\omega_{ce}} \left[ik_\parallel + \nabla_\parallel \ln \left(\frac{P_{e0} u_{\parallel e1}}{B^{5/2}} \right) \right] u_{\parallel e1} = ik_\theta \frac{e\phi_1}{m_e}, \quad (\text{III.5})$$

$$c_e^2 [ik_\parallel + \nabla_\parallel \ln h_{e1}] h_{e1} - i \frac{k_\theta c_e^2}{\omega_{ce}} [ik_\parallel + \nabla_\parallel \ln (\sqrt{B} u_{\perp e1})] u_{\perp e1} + i \frac{k_\perp c_e^2}{\omega_{ce}} [ik_\parallel + \nabla_\parallel \ln (\sqrt{B} u_{\theta e1})] u_{\theta e1} - i [\omega_\parallel + i\nu_e] u_{\parallel e1} = [ik_\parallel + \nabla_\parallel \ln \phi_1] \frac{e\phi_1}{m_e}. \quad (\text{III.6})$$

The inverse of the determinant of the matrix A_e of the above linear system, D_e , is

$$D_e = \omega_{ce}^2 (\omega_\parallel + i\nu_e) \left\{ \omega_e \left(1 - \frac{k^2 \rho_e^2}{2} \right)^2 - \frac{k_\theta c_e^2}{\omega_{ce}} \left(1 - \frac{k^2 \rho_e^2}{2} \right) \nabla_\perp \ln \left(\frac{n_0 u_{\perp e1}}{B h_{e1}} \right) + k^2 \rho_e^2 (\omega_\perp + i\nu_e) - \frac{\Omega_\parallel^2}{\omega_\parallel + i\nu_{\parallel e}} + \rho_e^2 k_\perp^2 \frac{k_\theta c_{e\perp}^2}{\omega_{ce}} \nabla_\perp \ln \left(\frac{u_{\perp e1}}{u_{\theta e1}} \right) + \omega_e O(\varepsilon) \right\}, \quad (\text{III.7})$$

where the frequency Ω_\parallel is defined as

$$\Omega_\parallel^2 = -c_e^2 \left[(ik_\parallel + \varkappa_\parallel + \varkappa_n) \left(1 + \frac{k^2 \rho_e^2}{2} \right) + \varkappa_T k^2 \rho_e^2 \right] \times \left[(ik_\parallel + \nabla_\parallel \ln h_{e1}) \left(1 - \frac{k^2 \rho_e^2}{2} \right) + ik_\parallel k^2 \rho_e^2 + \varkappa_\perp k_\theta^2 \rho_e^2 + \varkappa_\theta k_\perp^2 \rho_e^2 \right], \quad (\text{III.8})$$

with parallel gradients of zeroth-order terms

$$\varkappa_n = \nabla_\parallel \ln \left(\frac{n_0}{\sqrt{B}} \right), \quad \varkappa_T = \nabla_\parallel \ln \left(\frac{T_e}{\sqrt{B^3}} \right) \quad (\text{III.9})$$

and parallel gradients of unknown first-order terms

$$\varkappa_\perp = \nabla_\parallel \ln (\sqrt{B} u_{\perp e1}), \quad \varkappa_\theta = \nabla_\parallel \ln (\sqrt{B} u_{\theta e1}), \quad (\text{III.10})$$

$$\varkappa_\parallel = \nabla_\parallel \ln \left(\frac{u_{\parallel e1}}{\sqrt{B}} \right).$$

We can now compute h_{e1} keeping only $O(1)$ terms:

$$\frac{h_{e1}}{e\phi_1/m_e} = \frac{1}{c_e^2} \left\{ 1 - \frac{\omega_{ce}^2}{D_e} \left(1 - \frac{k^2 \rho_e^2}{2} \right) \left[(\omega_\parallel + i\nu_e) \times \left(\omega_e \left(1 - \frac{k^2 \rho_e^2}{2} \right) + \frac{k_\theta c_e^2}{\omega_{ce}} \nabla_\perp \ln \frac{h_{e1}}{\phi_1} \right) \right] - \omega_{ce}^2 \rho_e^2 \left[(\varkappa_\parallel + \varkappa_n) \left(1 - \frac{k^2 \rho_e^2}{2} \right) + (\varkappa_\parallel + \varkappa_n + \varkappa_T) k^2 \rho_e^2 \right] \nabla_\parallel \ln \frac{h_{e1}}{\phi_1} \right\}. \quad (\text{III.11})$$

Now, neglecting second order spatial derivatives, we can simplify the algebra that results by using the weakly inhomogeneous plasma assumption as in Eq. (II.11), from which $|\nabla \omega_{ce}| \gg |\nabla \omega_e|$. Then, from Eq. (III.7) the gradient of D_e can be approximated as

$$\nabla \ln D_e \simeq \nabla \ln \omega_{ce}^2 = 2\nabla \ln B. \quad (\text{III.12})$$

The gradient of $\ln h_{e1}$ can be obtained from differentiating Eq.

(III.11) as

$$\nabla \ln h_{e1} \simeq -\nabla \ln c_e^2 + \nabla \ln \phi_1 = \nabla \ln \frac{\phi_1}{T_e}. \quad (\text{III.13})$$

The identity (III.13), when substituted into Eq. (III.11), leads to the cancellation of the perpendicular derivatives of ϕ_1 , being $\nabla_\perp \ln (h_{e1}/\phi_1) = -\nabla_\perp \ln T_e$. By defining the following

frequencies:

$$\omega_{Te} \equiv -\frac{k_\theta c_e^2}{\omega_{ce}} \nabla_\perp \ln T_e, \quad (\text{III.14})$$

$$\begin{aligned} \sigma_\parallel^2 \equiv & c_e^2 \left(1 - \frac{k^2 \rho_e^2}{2}\right) \left[(\varkappa_\parallel + \varkappa_n) \left(1 - \frac{k^2 \rho_e^2}{2}\right) \right. \\ & \left. + (\varkappa_\parallel + \varkappa_n + \varkappa_T) k^2 \rho_e^2 \right] \nabla_\parallel \ln T_e, \end{aligned} \quad (\text{III.15})$$

Eq. (III.11) simplifies to

$$\begin{aligned} \frac{h_{e1}}{e\phi_1/m_e} = & \frac{1}{c_e^2} \left[1 + \frac{\omega_{ce}^2}{D_e} \sigma_\parallel^2 \right. \\ & \left. - \frac{\omega_{ce}^2}{D_e} \left(1 - \frac{k^2 \rho_e^2}{2}\right)^2 (\omega_\parallel + iv_e) \left(\omega_e + \frac{\omega_{Te}}{1 - k^2 \rho_e^2/2}\right) \right]. \end{aligned} \quad (\text{III.16})$$

The velocities yield (keeping only leading $O(1)$ terms)

$$\begin{aligned} \frac{u_{\perp e1}}{e\phi_1/m_e} = & -\frac{i\omega_{ce}}{D_e} \left(1 - \frac{k^2 \rho_e^2}{2}\right) (\omega_\parallel + iv_e) k_\theta \\ & \times \left(\omega_e + \frac{\omega_{Te}}{1 - k^2 \rho_e^2/2}\right) \end{aligned} \quad (\text{III.17})$$

$$\begin{aligned} \frac{u_{\theta e1}}{e\phi_1/m_e} = & \frac{i\omega_{ce}}{D_e} \left(1 - \frac{k^2 \rho_e^2}{2}\right) (\omega_\parallel + iv_e) k_\perp \\ & \times \left(\omega_e + \frac{\omega_{Te}}{1 - k^2 \rho_e^2/2}\right) \end{aligned} \quad (\text{III.18})$$

$$\begin{aligned} \frac{u_{\parallel e1}}{e\phi_1/m_e} = & -\frac{i\omega_{ce}^2}{D_e} \left(1 - \frac{k^2 \rho_e^2}{2}\right) \\ & \times \left[\left(ik_\parallel + \nabla_\parallel \ln \frac{\phi_1}{T_e}\right) \left(1 - \frac{k^2 \rho_e^2}{2}\right) + ik_\parallel k^2 \rho_e^2 \right. \\ & \left. + \varkappa_\perp k_\theta^2 \rho_e^2 + \varkappa_\theta k_\perp^2 \rho_e^2 \right] \left(\omega_e + \frac{\omega_{Te}}{1 - k^2 \rho_e^2/2}\right). \end{aligned} \quad (\text{III.19})$$

As in Eq. (III.13), Eqs. (III.17) to (III.19) allow us to compute the gradients of each velocity component neglecting second order spatial derivatives:

$$\nabla \ln u_{\perp e1} = \nabla \ln u_{\theta e1} = \nabla \ln \frac{\phi_1}{B}, \quad (\text{III.20})$$

$$\nabla \ln u_{\parallel e1} = \nabla \ln \phi_1. \quad (\text{III.21})$$

We can now rewrite h_{e1} , D_e and Ω_\parallel as functions of ϕ_1 and $\nabla \ln \phi_1$. The above relations imply that the parallel gradients of Eq. (III.10) are

$$\varkappa_\perp = \varkappa_\theta = \varkappa_\parallel = \nabla_\parallel \ln \frac{\phi_1}{\sqrt{B}}, \quad (\text{III.22})$$

while Ω_\parallel (Eq. (III.8)) becomes

$$\begin{aligned} \Omega_\parallel^2 = & -c_e^2 \left\{ \left(ik_\parallel + \nabla_\parallel \ln \frac{n_0 \phi_1}{B} - \frac{k^2 \rho_e^2/2}{1 + k^2 \rho_e^2/2} \nabla_\parallel \ln B \right) \left(1 + \frac{k^2 \rho_e^2}{2} \right) + k^2 \rho_e^2 \nabla_\parallel \ln \frac{T_e}{B} \right\} \\ & \times \left\{ \left(ik_\parallel + \nabla_\parallel \ln \frac{n_0 \phi_1}{B} - \frac{k^2 \rho_e^2/2}{1 + k^2 \rho_e^2/2} \nabla_\parallel \ln B - \nabla_\parallel \ln \frac{p_{e0}}{B} \right) \left(1 + \frac{k^2 \rho_e^2}{2} \right) + k^2 \rho_e^2 \nabla_\parallel \ln T_e \right\}. \end{aligned} \quad (\text{III.23})$$

The shape of $\nabla \ln \phi_1$ is selected so that the collisionless form of the dispersion relation appears as a real polynomial in ω_i . This is done so that the plasma inhomogeneities don't act as spurious sources or sinks of energy: Appendix B offers a more in-depth discussion supporting the above considerations. Then, by setting $\text{Im}\{\Omega_\parallel^2\} = 0$ we obtain

$$\nabla_\parallel \ln \frac{n_0 \phi_1}{B} = \frac{1}{2} \nabla_\parallel \ln \frac{p_{e0}}{B} - k^2 \rho_e^2 \nabla_\parallel \ln T_e \quad (\text{III.24})$$

so that Ω_\parallel^2 can be rewritten as

$$\begin{aligned} \Omega_\parallel^2 = & c_e^2 \left(1 + \frac{k^2 \rho_e^2}{2}\right)^2 \\ & \times \left\{ k_\parallel^2 + \frac{1}{4} \left[\nabla_\parallel \ln \frac{p_{e0}}{B} - \frac{k^2 \rho_e^2}{1 + k^2 \rho_e^2/2} \nabla_\parallel \ln B \right]^2 \right\} \end{aligned} \quad (\text{III.25})$$

while σ_\parallel^2 becomes

$$\begin{aligned} \sigma_\parallel^2 = & \frac{c_e^2}{2} \left(1 - \frac{k^4 \rho_e^4}{4}\right) \nabla_\parallel \ln T_e \\ & \times \left\{ \nabla_\parallel \ln \frac{p_{e0}}{B} + \frac{k^2 \rho_e^2}{1 + k^2 \rho_e^2/2} (3\nabla_\parallel \ln B + k^2 \rho_e^2 \nabla_\parallel \ln T_e) \right\}. \end{aligned} \quad (\text{III.26})$$

This procedure is not needed for the shape of $\nabla_{\perp} \ln \phi_1$, as it was canceled by combining Eqs. (III.11) and (III.13). By defining the frequency

$$\omega_{Me} \equiv -\frac{k_{\theta} c_e^2}{\omega_{ce}} \nabla_{\perp} \ln \frac{n_0}{B^2}, \quad (\text{III.27})$$

and recalling the definition of ω_{\perp} from Eq. (III.2), the determinant (Eq. (III.7)) can finally be rewritten as

$$D_e = \omega_{ce}^2 (\omega_{\parallel} + i\nu_e) \left\{ \omega_{Me} + \omega_{Te} + \omega_e \left(1 + \frac{k^4 \rho_e^4}{4} \right) + ik^2 \rho_e^2 \nu_e - \frac{\Omega_{\parallel}^2}{\omega_{\parallel} + i\nu_e} \right\} \quad (\text{III.28})$$

where we have discarded the $O(\varepsilon)$ terms. Eq. (III.16) becomes

$$h_{e1} = \frac{e\phi_1}{m_e c_e^2} \times \frac{\omega_{Me} + k^2 \rho_e^2 \left(\frac{\omega_{Te}}{2} + \omega_e + i\nu_e \right) - \frac{\Omega_{\parallel}^2 - \sigma_{\parallel}^2}{\omega_{\parallel} + i\nu_e}}{\omega_{Me} + \omega_{Te} + \omega_e \left(1 + \frac{k^4 \rho_e^4}{4} \right) + ik^2 \rho_e^2 \nu_e - \frac{\Omega_{\parallel}^2}{\omega_{\parallel} + i\nu_e}} \quad (\text{III.29})$$

and by coupling Eq. (III.29) with Eq. (II.12) through quasineutrality, dividing by ϕ_1 and keeping only $O(1)$ terms, we get the dispersion relation

$$\frac{k^2 c_s^2}{\omega_i^2} = \frac{\omega_{Me} + k^2 \rho_e^2 \left(\frac{\omega_{Te}}{2} + \omega_e + i\nu_e \right) - \frac{\Omega_{\parallel}^2 - \sigma_{\parallel}^2}{\omega_{\parallel} + i\nu_e}}{\omega_{Me} + \omega_{Te} + \omega_e \left(1 + \frac{k^4 \rho_e^4}{4} \right) + ik^2 \rho_e^2 \nu_e - \frac{\Omega_{\parallel}^2}{\omega_{\parallel} + i\nu_e}} \quad (\text{III.30})$$

with Ω_{\parallel} containing effects of both parallel wave propagation and gradients. As we will see later, σ_{\parallel} is negligible in most cases.

Eq. (III.30) is clearly akin to Eq. (31) from [23], with the additions of magnetic curvature effects, parallel dynamics and plasma inhomogeneities in the \perp - \parallel meridional plane and serves as the basis for the discussion in the rest of the paper.

A. Notable limits of the low frequency dispersion relation

From here, two notable limits can be taken: the dispersion relations for MSHI [23] and the MTSI [27], respectively

$$\frac{k^2 c_s^2}{\omega_i^2} = \frac{\omega_{Me}}{\omega_{Me} + \omega_{Te} + \omega_e} \quad (k^2 \rho_e^2 \rightarrow 0, \Omega_{\parallel} \rightarrow 0), \quad (\text{III.31})$$

and

$$\frac{k^2 c_s^2}{\omega_i^2} = -\frac{c_e^2 k_{\parallel}^2}{\omega_e^2 - c_e^2 k_{\parallel}^2} \quad (k^2 \rho_e^2 \rightarrow 0, \nabla Q_0 \rightarrow 0), \quad (\text{III.32})$$

both expressed in their quasineutral limit.

On the other hand, if we assume $\nabla_{\parallel} \ln Q_0 = 0$, $\nu_e \gg \omega_e$ and $k\rho_e \ll 1$, we recover

$$\frac{k^2 c_s^2}{\omega_i^2} = \frac{\omega_{Me} + i \left(k^2 \rho_e^2 \nu_e + c_e^2 k_{\parallel}^2 / \nu_e \right)}{\omega_{Me} + \omega_{Te} + \omega_e + i \left(k^2 \rho_e^2 \nu_e + c_e^2 k_{\parallel}^2 / \nu_e \right)} \quad (\text{III.33})$$

which is the cold, unmagnetized ion limit of Eq. (13) from [43].

The first two limits (III.31)-(III.32) express the two main ingredients for stream and drift-gradient instabilities, which are interspecies drifts due to gradients (in the perpendicular direction) or due to different thermal velocities (in the parallel direction), as will be later shown in section IV A. The third limit (III.33) shows how the combined presence of drifts and collisions naturally introduces destabilization in the problem by introducing imaginary terms in the dispersion relation, a concept further explored in section IV B. In summary, these three limits show the building blocks for fluid instabilities that arise in partially magnetized plasmas.

IV. LOW FREQUENCY INSTABILITIES

In general, solutions of the dispersion relation obtained in Eq. (III.30), $\omega_i = \omega_i(\mathbf{k})$, come in two regimes: a higher frequency pair of electron drift waves with $\omega_i \sim \mathbf{k} \cdot \mathbf{u}_{e0}$, and a lower-hybrid pair, with $\omega_i \sim k\rho_e \omega_{LH}$. This is a framework similar to that analysed in [11] for the ‘low-frequency modes in the low-drift regime’, with an added fourth branch due to the inclusion of parallel dynamics.

In the collisionless limit, the lower-hybrid branches experience destabilization in the form of a reactive instability (pair of complex conjugate solutions). The reason, as anticipated in the introduction, has to do with the existence of ‘slow’ negative energy waves in presence of zeroth-order drifts. In the collisionless case the only energy sinks present in the plasma are ‘fast’ positive energy waves: when the two types of wave have matching frequencies and wavenumbers, an unstable interaction takes place [44]. In the collisional case, no reactive interaction is needed. When inelastic collisions are present in the medium they act as an energy sink, destabilizing the slow wave without the need of coupling with the fast wave.

In general, the presence of collisions widens considerably the parametric instability region, while at the same time lowering the growth rates of the drift gradient instabilities identified in the collisionless limit. The analysis is therefore focused mostly on drift-gradient (collisionless) instabilities; notwithstanding this, at the end of this section, a paragraph is dedicated to drift-resistive (collisional) instability conditions and how resistive effects alter the collisionless case.

A. Drift-gradient instabilities

Defining:

$$\Delta \equiv \omega_i - \omega_e = \mathbf{k} \cdot (\mathbf{u}_{e0} - \mathbf{u}_{i0}), \quad \Delta_{\parallel} \equiv \omega_i - \omega_{\parallel}, \quad (\text{IV.1})$$

the former being the Doppler shift between the two species, and the latter being the interspecies Doppler shift accounting for gyroviscous cancellation, Eq. (III.30) can be hugely simplified by considering either electron drift wave solutions $\omega_i^2 \sim \Delta^2 \gg k^2 c_s^2$ or lower-hybrid wave solutions $\omega_i^2 \sim k^2 c_s^2 = k^2 \rho_e^2 \omega_{LH}^2$. Here we are assuming $|u_{e0}| \gg |c_s|$, as expected in many current-free MNs. Additionally we will assume $\Omega_{\parallel}^2 \gg \sigma_{\parallel}^2$ being $|\nabla_{\parallel} \ln p_{e0}| \gg |\nabla_{\parallel} \ln T_e|$, as justified in Table V.1.

For the electron drift wave solutions, Eq. (III.30) approximately becomes

$$\omega_e^2 + \left(\frac{\omega_{Me}}{k^2 \rho_e^2} + \frac{\omega_{Te}}{2} + \Delta - \Delta_{\parallel} \right) \omega_e + (\Delta - \Delta_{\parallel}) \left(\frac{\omega_{Me}}{k^2 \rho_e^2} + \frac{\omega_{Te}}{2} \right) - \frac{\Omega_{\parallel}^2}{k^2 \rho_e^2} \simeq 0 \quad (\text{IV.2})$$

admitting solutions

$$\omega_i = \Delta - \frac{1}{2} \left(\frac{\omega_{Me}}{k^2 \rho_e^2} + \frac{\omega_{Te}}{2} + \Delta - \Delta_{\parallel} \right) \times \left[1 \pm \frac{\sqrt{[k^2 \rho_e^2 (\Delta - \Delta_{\parallel} - \omega_{Te}/2) - \omega_{Me}]^2 + \Omega_{\parallel}^2}}{k^2 \rho_e^2 (\Delta - \Delta_{\parallel} + \omega_{Te}/2) + \omega_{Me}} \right], \quad (\text{IV.3})$$

which are always stable.

Moving to the lower-hybrid branches, following the assumption $k^2 c_s^2 \ll \Delta^2$ and expanding up to the second power of ω_i/Δ , we get

$$\omega_i^2 - \frac{k^2 c_s^2 \omega_i (\Delta + \Delta_{\parallel}) (1 + k^4 \rho_e^4/4) - \omega_{Me} - \omega_{Te}}{\Delta_{\parallel} \omega_{Me} + k^2 \rho_e^2 (\omega_{Te}/2 - \Delta) + \Omega_{\parallel}^2/\Delta_{\parallel}} - k^2 c_s^2 \frac{\Delta (1 + k^4 \rho_e^4/4) - \omega_{Me} - \omega_{Te} - \Omega_{\parallel}^2/\Delta_{\parallel}}{\omega_{Me} + k^2 \rho_e^2 (\omega_{Te}/2 - \Delta) + \Omega_{\parallel}^2/\Delta_{\parallel}} \simeq 0 \quad (\text{IV.4})$$

whose solution $\omega_i = \omega_{ri} + i\gamma$ has real and imaginary parts:

$$\omega_{ri} = k^2 \rho_e^2 \frac{\omega_{LH}^2 (\Delta + \Delta_{\parallel}) (1 + k^4 \rho_e^4/4) - \omega_{Me} - \omega_{Te}}{2\Delta_{\parallel} \omega_{Me} + k^2 \rho_e^2 (\omega_{Te}/2 - \Delta) + \Omega_{\parallel}^2/\Delta_{\parallel}}, \quad (\text{IV.5})$$

$$\gamma \simeq \omega_{LH} k \rho_e \sqrt{\frac{\Delta (1 + k^4 \rho_e^4/4) - \omega_{Me} - \omega_{Te} - \Omega_{\parallel}^2/\Delta_{\parallel}}{\omega_{Me} + k^2 \rho_e^2 (\omega_{Te}/2 - \Delta) + \Omega_{\parallel}^2/\Delta_{\parallel}}}. \quad (\text{IV.6})$$

The expression for γ allows us to retrieve the following gen-

eral instability criterion:

$$\left[\Delta \left(1 + \frac{k^4 \rho_e^4}{4} \right) - \omega_{Me} - \omega_{Te} - \frac{\Omega_{\parallel}^2}{\Delta_{\parallel}} \right] \times \left[\omega_{Me} + k^2 \rho_e^2 \left(\frac{\omega_{Te}}{2} - \Delta \right) + \frac{\Omega_{\parallel}^2}{\Delta_{\parallel}} \right] > 0. \quad (\text{IV.7})$$

This relation underlines how the electron drifts in the ion reference frame are the ones driving the instability, whether they may be due to *a*) gradients in electrostatic potential, pressure or magnetic field, or *b*) thermal motion along the magnetic field lines.

1. Long-wavelength limit

Taking the limit $k\rho_e \rightarrow 0$ of relation (IV.7), the instability criterion simplifies to:

$$\left[\Delta - \omega_{Me} - \omega_{Te} - \frac{\Omega_{\parallel}^2}{\Delta_{\parallel}} \right] \left[\omega_{Me} + \frac{\Omega_{\parallel}^2}{\Delta_{\parallel}} \right] > 0. \quad (\text{IV.8})$$

This expression can be easily shown to be a generalization of the MSHI and the MTSI conditions, Eqs. (III.31)-(III.32). Neglecting parallel propagation and gradients, $\Omega_{\parallel} = 0$, Eq. (IV.8) yields the MSHI criterion

$$(\Delta - \omega_{Me} - \omega_{Te}) \omega_{Me} > 0. \quad (\text{IV.9})$$

Instead, dropping perpendicular inhomogeneities ($\omega_{Me} = 0$, $\Delta_{\parallel} = \Delta$) Eq. (IV.8) yields the MTSI condition

$$\Delta^2 > \Omega_{\parallel}^2. \quad (\text{IV.10})$$

2. Finite Larmor radius effects

As $k\rho_e$ becomes non-negligible, rearranging the relation (IV.7) yields a finite Larmor radius correction to the criterion in (IV.8):

$$\left[\Delta - \omega_{Me} - \omega_{Te} - \frac{\Omega_{\parallel}^2}{\Delta_{\parallel}} \right] \left[\omega_{Me} + \frac{\Omega_{\parallel}^2}{\Delta_{\parallel}} \right] > -k^2 \rho_e^2 \left[\left(\frac{\omega_{Te}}{2} - \Delta \right) \left(\Delta - \omega_{Me} - \frac{\Omega_{\parallel}^2}{\Delta_{\parallel}} \right) + \Delta \left(\omega_{Me} + \frac{\Omega_{\parallel}^2}{\Delta_{\parallel}} \right) \frac{k^2 \rho_e^2}{4} + \Delta \left(\frac{\omega_{Te}}{2} - \Delta \right) \frac{k^4 \rho_e^4}{2} \right], \quad (\text{IV.11})$$

implying that even if the condition for long-wavelength instabilities is not respected (for instance, left-hand side of (IV.11) < 0), we can still have an onset for larger values of the normalized wavenumber $k\rho_e$. On the other hand, if the long-wavelength criterion from (IV.8) is satisfied, higher values of $k^2 \rho_e^2$ might cause ω_i to become real, quenching the instability.

B. Drift-resistive instabilities

When collisional effects are included, the dispersion relation becomes a complex polynomial in ω_i , yielding in general complex solutions as a result.

Using analytical continuation:

$$0 \simeq \frac{\partial f}{\partial \omega_i} \delta \omega_i + \frac{\partial f}{\partial v_e} v_e, \quad (\text{IV.12})$$

yields the growth rate due to destabilization from dissipative forces:

$$\delta \omega_i = - \left. \frac{\partial f / \partial v_e}{\partial f / \partial \omega_i} \right|_{v_e=0} v_e. \quad (\text{IV.13})$$

Computing the partial derivatives, and substituting them into Eq. (IV.13):

$$\begin{aligned} \delta \omega_i = & -i v_e (\omega_i^2 - k^2 c_s^2) \left(k^2 \rho_e^2 + \frac{\Omega_{\parallel}^2}{\omega_{\parallel}^2} \right) \\ & \times \left\{ 2 \omega_i \left[\omega_{Me} + k^2 \rho_e^2 \left(\frac{\omega_{Te}}{2} + \omega_e \right) - \frac{\Omega_{\parallel}^2}{\omega_{\parallel}^2} \right] \right. \\ & \left. + \left(k^2 \rho_e^2 + \frac{\Omega_{\parallel}^2}{\omega_{\parallel}^2} \right) (\omega_i^2 - k^2 c_s^2) - k^2 c_s^2 \left(1 - \frac{k^2 \rho_e^2}{2} \right)^2 \right\}^{-1}. \end{aligned} \quad (\text{IV.14})$$

For our high-drift case of interest, long wavelength ($k\rho_e \rightarrow 0$) lower-hybrid drift waves $|\omega_i| \sim kc_s \ll \Delta$ can be shown to be destabilized when

$$\omega_i \omega_{Me} (\omega_i^2 - k^2 c_s^2) < 0, \quad (\text{IV.15})$$

which is always true for one of the two branches. It can also be shown through Eq. (IV.14) that drift gradient instability growth rates are in general lowered by the added dissipation. From this, we can state that while collisions offer a more general destabilization criterion, they also tend to reduce unstable growths excited by gradients alone.

V. APPLICATION TO A MAGNETIC NOZZLE PLUME

As a means of illustration, numerical solutions of (III.30) are obtained for each point in the entire 2D map shown in Figure V.1, stemming from the simulations of the MN of a helicon plasma thruster reported in [37]. The simulation data was obtained through a 2D hybrid code, HYPHEN-EPT, with electrons modelled as a magnetized diffusive fluid, while the heavy species are simulated through a PIC formulation[45, 46], and wavefields are solved in the frequency domain using a cold-plasma-wave model [37]. What we show here is a subset of the entire simulation domain, the latter including the plume up to a length of 40 cm, a radius of 18 cm, and the ionization chamber as well.

The region shown in Figure V.1 only covers the MN region directly downstream of the simulated HPT, whose exit is situated at the axial coordinate $z = 0$ and extends from $r = 0$

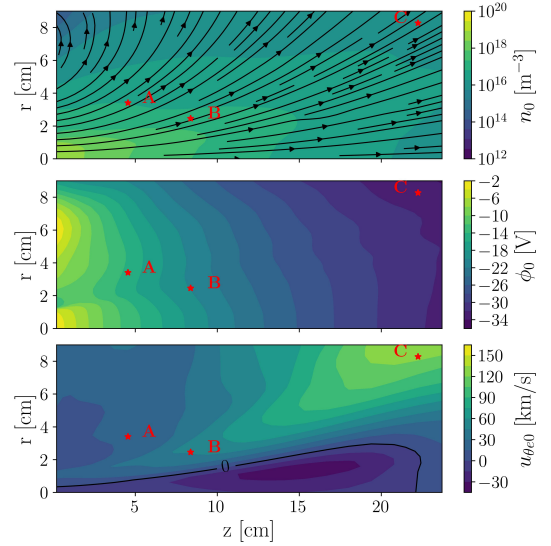


FIG. V.1. Contour plots for n_0 , ϕ_0 and $u_{\theta e0}$, for the simulation data of the plasma expansion in the magnetic nozzle of a helicon plasma thruster, from Ref. [37]. Red dots indicate the three points for which a dedicated ω_i - k analysis is presented in subsequent figures. In the plot of n_0 , \mathbf{B} streamlines have been superimposed.

up to the radial coordinate $r = 1.25$ cm. Three representative points have been chosen from the shown MN region, two in the near-plume and one in the far-plume part of the discharge, to show three different $\omega(\mathbf{k})$ trends for a drift-gradient instability in the laboratory frame, with $\omega = \omega_i + \mathbf{k} \cdot \mathbf{u}_{i0}$. Point A presents gradients oriented for the most part in the perpendicular direction, with parallel gradients which are of the $O(c_s/c_e)$ order with respect to the perpendicular ones, and $\nabla_{\perp} \phi \nabla_{\perp} (n_0/B^2) < 0$, a condition necessary for MSHI as expressed in Eq. (IV.9); point B still presents mainly perpendicular gradients but with $\nabla_{\perp} \phi \nabla_{\perp} (n_0/B^2) > 0$; point C, on the other hand, presents parallel gradients which are of order greater than $O(c_s/c_e)$ with respect to the perpendicular ones, thus making the parallel dynamics effect the dominant ones in the dispersion relation. Each location shows a different evolution of the growth rate γ as a function of k_{θ} , starting from the triggering of a quasi-MSHI in the first case and ending with a short-wavelength instability, mostly driven by parallel dynamics, in the third case. Table V.1 shows their coordinates, and associated zeroth-order plasma quantities and gradients.

Figure V.2 presents the real and imaginary parts of the solution $\omega(\mathbf{k})$ for the near-plume point A with axial and radial coordinates $(z, r) = (4.5, 3.4)$ cm. For $k_{\parallel}/k_{\theta} = k_{\perp}/k_{\theta} = 0$ it presents an instability mainly driven by perpendicular dynamics, respecting the MSHI criterion from Eq. (IV.9) and developing mostly in long-wavelength regime, $k\rho_e \ll 1$. The instability quenches for small values of the ratio k_{\parallel}/k_{θ} ; the effect of k_{\perp} is, on the other hand, negligible for values of k_{\perp}/k_{θ} of interest, leaving the shape of the solution almost unchanged. For this very reason, in this point and in the following ones, the solutions have been plotted with $k_{\perp}/k_{\theta} = 0$.

Figure V.3 shows the destabilized lower-hybrid branch for the point B with $(z, r) = (8.4, 2.5)$ cm. In this case, the MSHI

Points	z [cm]	r [cm]	ω_{LH} [10^6 s^{-1}]	c_s [10^3 m/s]	$u_{\theta e0}$ [10^5 m/s]	$\nabla_{\perp} \ln n_0$ [m^{-1}]	$\nabla_{\perp} \ln B$ [m^{-1}]	$\nabla_{\perp} \ln T_e$ [m^{-1}]	$\nabla_{\parallel} \ln (p_{e0}/B)$ [m^{-1}]	$\nabla_{\parallel} \ln T_e$ [m^{-1}]
A	4.5	3.4	8.1	1.9	1.7	-39.4	7.5	-2.5	0.4	-0.0
B	8.4	2.5	3.2	1.9	4.5	-98.7	2.5	3.2	-1.9	-0.2
C	22.2	8.3	0.2	1.8	12.8	-32.3	0.6	1.3	-3.4	-0.6

TABLE V.1. Coordinates, zeroth-order plasma quantities and gradients at the three reference points indicated in figure V.1.

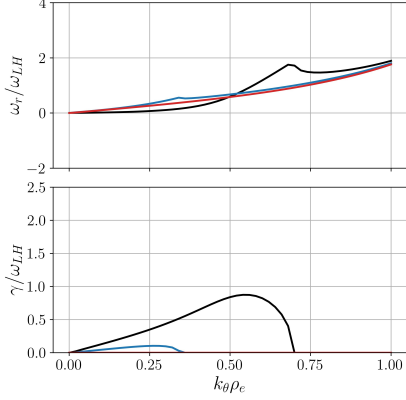


FIG. V.2. Real frequency (top figure) and growth rate (bottom figure) for the long-wavelength destabilization of the lower-hybrid branch for the point A of coordinates $(z, r) = (4.5, 3.4)$ cm. Black lines are for $k_{\parallel} = 0$; blue lines for $k_{\parallel}/k_{\theta} = 4 \cdot 10^{-3}$; red lines for $k_{\parallel}/k_{\theta} = 8 \cdot 10^{-3}$. Relevant zeroth-order plasma quantities and gradients are shown in Table V.1.

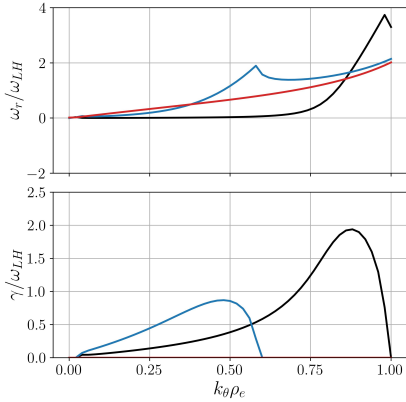


FIG. V.3. Real frequency (top figure) and growth rate (bottom figure) for the destabilized lower-hybrid branch for the point B of coordinates $(z, r) = (8.4, 2.5)$ cm, with onset in the long-wavelength regime and peak in the short-wavelength regime. Black lines are for $k_{\parallel} = 0$; blue lines for $k_{\parallel}/k_{\theta} = 2 \cdot 10^{-2}$; red lines for $k_{\parallel}/k_{\theta} = 4 \cdot 10^{-2}$. Relevant zeroth-order plasma quantities and gradients are shown in Table V.1.

is no longer respected as the perpendicular components of the electric field and density gradient have different sign, so that the inclusion of parallel dynamics is responsible for the destabilization of the lower-hybrid branch. The instability develops at a slight larger $k\rho_e$ but still in the long-wavelength regime. However its peak is reached in the short-wavelength,

at $k\rho_e = O(1)$. Once again, $|k_{\parallel}| > 0$ has a stabilizing effect.

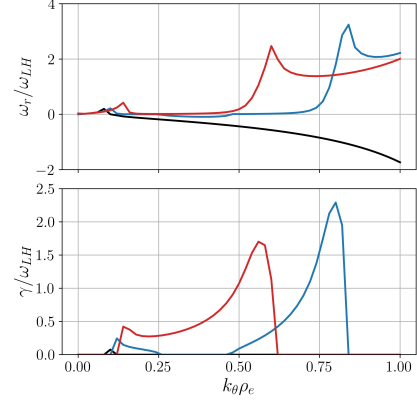


FIG. V.4. Real frequency (top figure) and growth rate (bottom figure) for the short-wavelength destabilization of the lower-hybrid branch for the point C of coordinates $(z, r) = (22.2, 8.3)$ cm. Black lines are for $k_{\parallel} = 0$; blue lines for $k_{\parallel}/k_{\theta} = 1.6 \cdot 10^{-1}$; red lines for $k_{\parallel}/k_{\theta} = 2 \cdot 10^{-1}$. Solutions with $\omega_r < 0$ are equivalent to solutions with $\omega_r > 0$ but opposite sign of k_{θ} . Relevant zeroth-order plasma quantities and gradients are shown in Table V.1.

Figure V.4 shows the (ω_i, k) plot of the unstable lower-hybrid branch at the point C with $(z, r) = (22.2, 8.3)$ cm. In this case, far from the MSHI condition and dominated by parallel dynamics, the term $\Omega_{\parallel}^2/\Delta_{\parallel}$ for $k_{\parallel}/k_{\theta} = 0$ (black line) gets cancelled by the large Doppler shift $\Delta \sim k_{\theta} u_{\theta e0}$, as shown by the small growth rate peak. The instability is then driven by finite parallel propagation $|k_{\parallel}/k_{\theta}| > 0$, creating a separate short-wavelength onset region as the ratio $|k_{\parallel}/k_{\theta}|$ grows (blue line). Eventually, the long and short-wavelength onset regions collapse into a single one for larger values of said ratio (red line).

These three cases have been analyzed to apply the concepts and criteria developed in section IV on a relevant configuration. To summarize, various regimes exist in the MN, and fluid waves can be destabilized by either perpendicular gradients, parallel dynamics (gradients and/or wave propagation) or a combination of the the above. The sign of the different perpendicular gradients can be used to assess which kind of mechanism is causing the instability to take place. Gyroviscous effects play a role as well, destabilizing or quenching pre-existing instabilities.

We may now move our attention on the study and identification of the most unstable modes developing at each point of a MN, as predicted by our model. For each point of the map, the maximum growth rate $\gamma_{max} = \max(\gamma(\mathbf{k}, \omega_r))$ has been obtained, with the associated wavenumber and real fre-

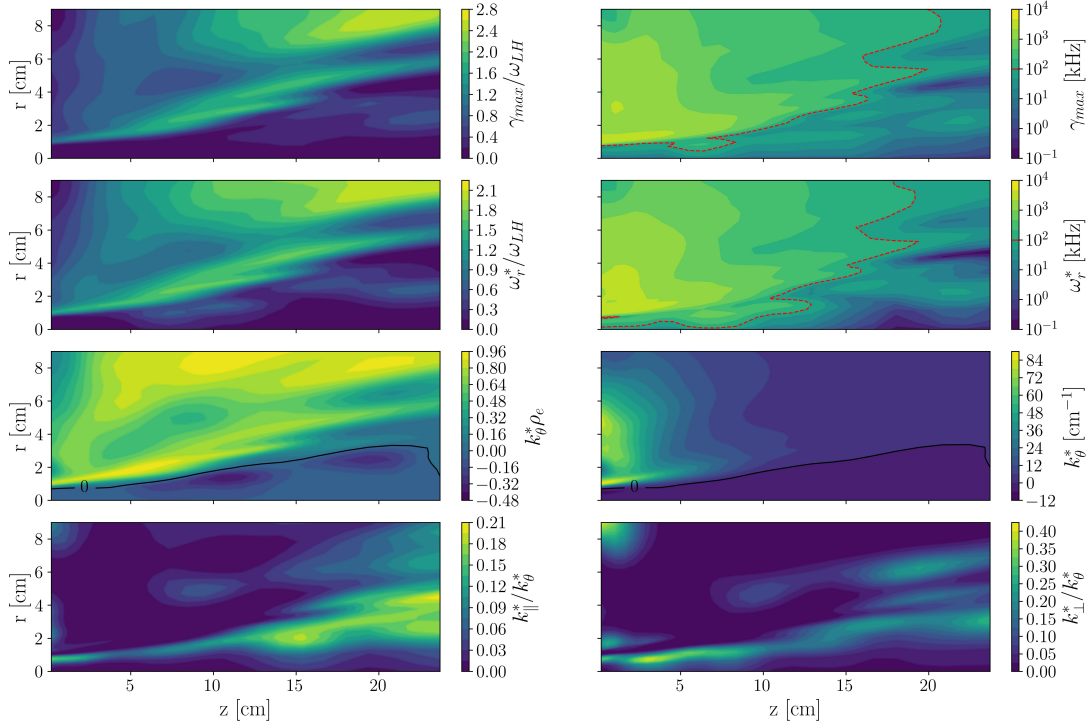


FIG. V.5. 2D maps of γ_{max} , ω_r^* , k_θ^* and k_\perp^* resulting from a point-wise local analysis across the MN plume region in the collisionless limit. The dashed red line in the plots of γ_{max} and ω_r^* represents the 100 kHz line.

quency in the laboratory frame k_\perp^* , ω_r^* respecting the conditions $\rho_e k_{\perp,\theta}^* < 1$ and $|k_{\parallel}^* c_e| < |\omega_e^*|$. The mode associated with $\gamma = \gamma_{max}$ is then the most unstable one for that particular point of the MN; 2D maps of γ_{max} , ω_r^* and k_θ^* are shown in Figure V.5. The condition needed for our cartesian expansion to be valid, i.e. $|rk_\theta| \gg 1$, will be relaxed to study points close to the axis.

The regions with larger γ_{max}/ω_{LH} are mostly found in those same points where $|u_{\theta e0}|$ reaches its peak values, as it can be seen comparing γ_{max} from Figure V.4 with the ones from Figures V.2 and V.3. This can be explained by looking at the relation between γ and Δ from Eq. (IV.6), with

$$\gamma \simeq kc_s \sqrt{\frac{\Delta - \omega_{Me} - \Omega_{\parallel}^2/\Delta_{\parallel}}{\omega_{Me} + \Omega_{\parallel}^2/\Delta_{\parallel}}}.$$

A similar consideration can be done with the plot of ω_r^* , recalling the expression of ω_r from Eq. (IV.5), and with the plot of $k_\theta^* \rho_e$, as $\Delta \propto k_\theta$. All these first three plots show very similar trends, as they all share a direct correlation with the Doppler shift Δ and the zeroth-order electron drift velocity $u_{\theta e0}$. The ratio $k_{\parallel}^*/k_\theta^*$ is quite negligible in the near-plume region. As we've stated in the discussion of the three (ω_r, k) plots, in this region the effect of a finite parallel propagation is, in general, to stabilize the wave. This is not true in the regions where the perpendicular gradients get close to 0, that is, closer to the axis and in the far-plume region, as shown in Figure V.4 and in Table V.1. The role of k_\perp^* , on the other hand, is quite marginal, as we've stated beforehand. It follows a trend more

or less similar to that of k_{\parallel}^* , peaking in a region of small γ_{max} . In those points where γ_{max} is reached for $k^* \rho_e = 1$, a kinetic formulation of the problem would be more suitable.

Most of the instabilities and their associated real frequencies fall in the 1 kHz–1 MHz range, decreasing as we move from the near-plume to far-plume region of the discharge. The modes with larger γ_{max} have a mainly-azimuthal associated wavenumber, $k^* \simeq k_\theta^* \mathbf{1}_\theta$.

Noticeably, the inclusion of parallel gradients in the dispersion relation plays a major role in the stability of the solution. Their presence allows the onset of instabilities in those points of the MN where the MSHI criterion from Eq. (IV.9) does not hold, even without $k_{\parallel} \neq 0$. This statement is further illustrated by the plots of Figure V.6, which have been computed by using a form of Eq. (III.30) *without* parallel gradients, $\nabla_{\parallel} \ln Q = 0$. These plots present a substantially different map for γ_{max} , with the majority of the instabilities taking place in those regions satisfying the MSHI criterion. The map of k_θ^* shows milder peaks, loosely following the ones of γ_{max} . k_{\parallel}^* has a much more prominent role in the onset of instabilities: this is due to the fact that, in the absence of parallel gradients, $\Omega_{\parallel}^2 \propto k_{\parallel}^2$. In the regions where the MSHI criterion is not satisfied, then, instabilities can only be driven by finite parallel propagation i.e. $k_{\parallel} \neq 0$. It is therefore clear that parallel gradients of plasma quantities have to be retained in the formulation to consistently include the complete set of mechanisms which lead to linear fluid instabilities of the plasma in the LF regime. The present work, to our knowledge, is the first to include said gradients.

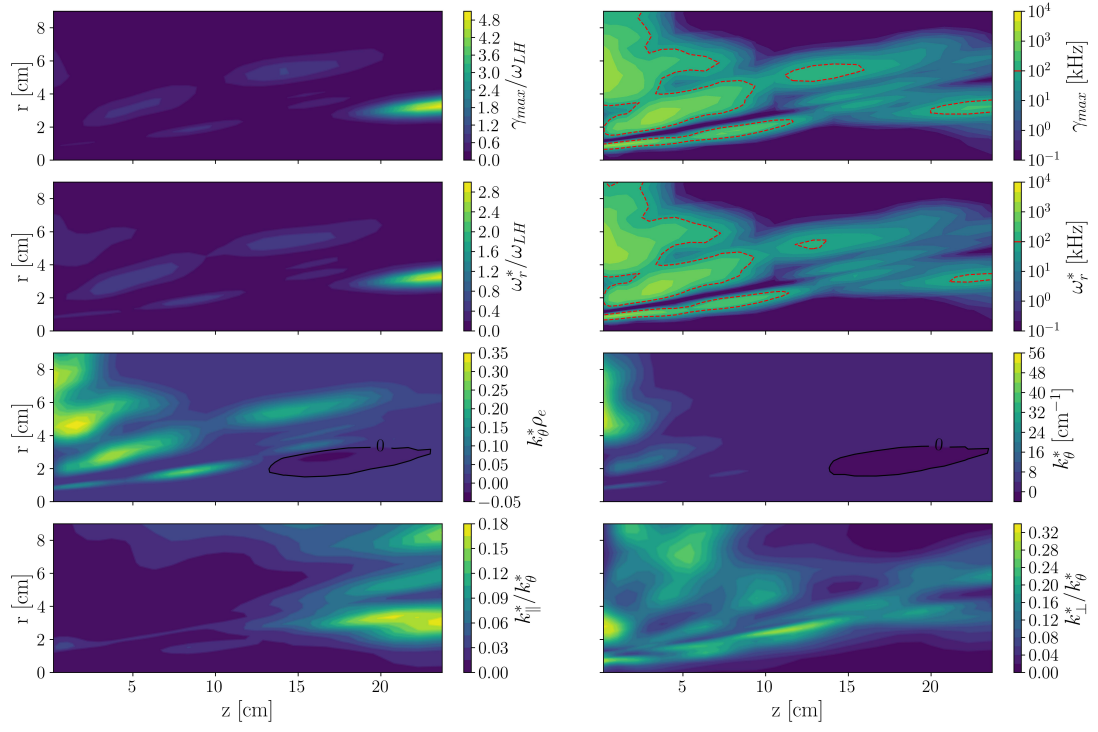


FIG. V.6. Similar to figure V.5, but removing parallel gradient effects in the dispersion relation.

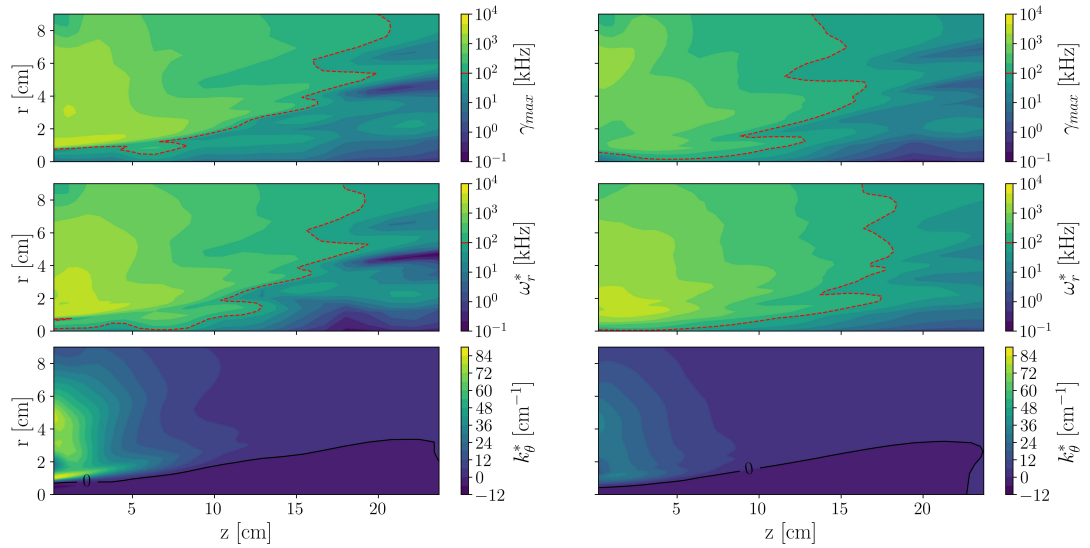


FIG. V.7. Similar to figure V.5, but including collisions. Left column with ν_e obtained directly from simulation; right column with ν_e artificially increased by a factor of 10^4 .

The effect of collisions on the instability peaks are negligible, as electron-neutral collision frequencies remain in the order $\nu_e \leq O(\omega_{LH})$, barely affecting the $O(\omega_{LH})$ growth rates. Overall, the 2D maps of γ_{max} , ω_r^* and k^* remain almost unchanged between the collisionless to the collisional case, as the most unstable modes are of the drift-gradient type. Figure V.7 compares two collisional cases, the first where the collisional frequency is directly obtained from the simulation data, and in the second case the same frequency is multiplied by a factor of 10^4 . Collisions show to have an effect only in those regions where drift gradient instabilities are minor or completely absent, slightly extending the regions of instability and slightly reducing the peak of gradient-driven growth rates.

We conclude this section with a qualitative comparison with the limited available experimental data. Recalling Figure V.5, we have shown that the most unstable modes predicted by our model consist of mainly-azimuthal waves with associated real oscillation frequency ω_r^* in the 1 kHz–1 MHz range. While Hepner et al.[31] and Vinci[32] do find fluctuations in a similar frequency range in the MN of their respective devices, they both describe waves with combined axial-azimuthal propagation (where the presence of a large k_{\parallel} introduces kinetic effects which elude our fluid model). Indeed, Hepner et al. attribute their observed fluctuations to an LHDI and invoke a kinetic formulation to justify it, involving values of parallel wavenumber comparable to the one in the azimuthal direction. In the works of both Takahashi et al.[28] and Maddaloni et al.[30], fluctuations are detected in their respective MNs, which fall in the 10–100 kHz range and consist of mostly azimuthal waves. Takahashi et al. identify their oscillations with azimuthal magnetosonic waves, while Maddaloni et al. present the case that the fluctuation spectrum they observe is due to a nonlinear parametric decay instability of the pump wave at 13.56 MHz, as the conditions for LHDI are not met where said fluctuations are observed. Our work suggests that an alternative explanation to either of them could be that the observed fluctuations are the signature of low frequency, drift-gradient instabilities of the type described above, which can be triggered even in those regions where the MSHI criterion is not satisfied, and the parallel wavenumber is too close to zero to justify the onset of MTSI.

VI. QUASI-LINEAR CROSS-FIELD TRANSPORT

In the collisionless case, the electron cross-field current at the zeroth order is null. This allows instability-driven electron transport to be a dominant term in this direction. To tackle the effect of linear perturbations on cross-field electron transport we quantify, through a limited quasi-linear analysis, when and how the non-linear interaction between these oscillations can produce a non-zero second order term in the electron current field.

These second order terms are generally comprised of a quasi-DC axisymmetric part, varying in time as $2\gamma t$, and a double frequency part. Since we want to gauge how instabilities affect the equilibrium over time, it is only the quasi-DC

part that we are interested in. For this purpose, we consider our plasma quantities to be comprised of an additional, quasi-DC and axisymmetric second order term, their expression now being

$$Q(\mathbf{x}, t) = Q_0(\mathbf{x}) + \frac{1}{2}[Q_1(\mathbf{x}) \exp(i\mathbf{k} \cdot \mathbf{x} - i\omega t) + CC] + Q_2(\mathbf{x}) \exp(2\gamma t) + \dots \quad (\text{VI.1})$$

We note that this expansion is not uniformly valid for all times; the second-order term will eventually result in a modified equilibrium solution, requiring the redefinition of Q_0 . In the following, we implicitly restrict our analysis to the time interval of validity of this expansion.

For the cross-field transport, we are interested in the second order, quasi-DC, perpendicular electron flux, which is given by:

$$(n_e u_{\perp e})_2 = n_0 \langle u_{\perp e1} h_{e1}^* \rangle \exp(-2\gamma t) + n_0 u_{\perp e2}. \quad (\text{VI.2})$$

Here, the quasi-DC, real part of the product two generic first-order quantities, say a_1 and b_1 , is

$$\langle a_1 b_1^* \rangle = \frac{a_1 b_1^* + a_1^* b_1}{4} \exp(2\gamma t). \quad (\text{VI.3})$$

The $\langle u_{\perp e1} h_{e1}^* \rangle$ term on the right-hand side of Eq. (VI.2) can be computed by substituting for $u_{\perp e1}$ the expression from (III.17)

$$u_{\perp e1} = - \frac{ik_{\theta}}{\omega_{ce}} \left(\omega_e + \frac{\omega_{Te}}{1 - k^2 \rho_e^2 / 2} \right) \left(1 - \frac{k^2 \rho_e^2}{2} \right) \frac{e\phi_1}{\omega_e \left(1 - \frac{k^2 \rho_e^2}{2} \right)^2 + \omega_{Me} + k^2 \rho_e^2 \left(\frac{\omega_{Te}}{2} + \omega_e \right) - \frac{\Omega_{\parallel}^2}{\omega_{\parallel}}} m_e;$$

making use of the LF dispersion relation (Eq. (III.30)), the expression for $\langle u_{\perp e1} h_{e1}^* \rangle$ renders as

$$\langle u_{\perp e1} h_{e1}^* \rangle = - \frac{k_{\theta} / \omega_{ce}}{1 - k^2 \rho_e^2 / 2} \left\langle i \left(\frac{e\phi_1}{m_e} - \frac{k^2 c_s^2 e\phi_1}{\omega_i^2 m_e} \right) h_{e1}^* \right\rangle = c_e \frac{k_{\theta} \rho_e}{1 - k^2 \rho_e^2 / 2} \left(\frac{kc_s}{\omega_{ri}^2 + \gamma^2} \right)^2 \omega_{ri} \gamma \frac{e^2 |\phi_1|^2}{T_e^2} \exp(2\gamma t). \quad (\text{VI.4})$$

In the last passage, we have used $h_{e1} = h_{i1} = k^2 c_s^2 e\phi_1 / T_e$, from Eq. (II.12).

The quasi-DC second order cross-field velocity $u_{\perp e2}$ can be obtained from the second order momentum equation (II.2):

$$2\gamma \mathbf{u}_{e2} + \mathbf{u}_{e0} \cdot \nabla \mathbf{u}_{e2} + \mathbf{u}_{e2} \cdot \nabla \mathbf{u}_{e0} + \langle \mathbf{u}_{e1} \cdot \nabla \mathbf{u}_{e1}^* \rangle \exp(-2\gamma t) = - \frac{\nabla p_{e2}}{m_e n_0} - \frac{\nabla \cdot \Pi_{e2}}{m_e n_0} + \frac{e \nabla \phi_2}{m_e} + \omega_{ce} \mathbf{1}_{\parallel} \times \mathbf{u}_{e2} - \left(\frac{\nabla p_{e0}}{m_e n_0} + \frac{\nabla \cdot \Pi_{e0}}{m_e n_0} \right) (\langle h_{e1} h_{e1}^* \rangle \exp(-2\gamma t) - h_{e2}) + \left\langle \left(\frac{\nabla p_{e1}}{m_e n_0} + \frac{\nabla \cdot \Pi_{e1}}{m_e n_0} \right) h_{e1}^* \right\rangle \exp(-2\gamma t), \quad (\text{VI.5})$$

where we have used the expansion $(n^{-1}Q)_2 = n_0^{-1}(Q_2 - Q_1 n_1 + Q_0 n_1^2 n_0^{-1} - Q_0 n_2) \exp(2\gamma t)$. In the LF regime $\gamma = O(\varepsilon \omega_{ce})$, so that the left-hand side of the above equation, i.e. the inertia, is of order ε with respect to the right-hand side. The perpendicular velocity $u_{\perp e2}$ is then obtained from the magnetic force term in the azimuthal momentum equation. Using $\nabla_{\theta} Q_0 = 0$ and $\nabla_{\theta} Q_2 = 0$ and Eq. (A.5) (yielding $\nabla \cdot \Pi_{e2} = O(n_0 m_e \omega_{ce} u_{\perp e2} \varepsilon)$), Eq. (VI.5) gets rewritten as

$$\omega_{ce} u_{\perp e2} \exp(2\gamma t) = - \left\langle \left(ik_{\theta} c_e^2 h_{e1} + \omega_{ce} \frac{k^2 \rho_e^2}{2} u_{e\perp 1} \right) h_{e1}^* \right\rangle (1 + O(\varepsilon)). \quad (\text{VI.6})$$

Having assumed isothermal perturbations, $T_{e1} = 0$, a reasonable assumption for low frequency oscillations [26], the contribution of pressure to second order cross-field flow is null. This only leaves the contribution from the product between the first-order divergence of the gyroviscous tensor from Eq. (A.3) and the first-order number density. This term is the second one appearing in the right hand side of Eq. (VI.6), and unlike inertial terms yields a contribution of order $O(k^2 \rho_e^2)$ with respect to the magnetic force. By making use of Eq. (VI.4) and $c_s = \rho_e \omega_{LH}$ and neglecting $O(\varepsilon)$ terms, we obtain the second order electron cross-field velocity

$$u_{\perp e2} = -c_e \rho_e \omega_{LH}^2 \frac{k^4 \rho_e^4 / 2}{1 - k^2 \rho_e^2 / 2} \frac{k_{\theta} \omega_{ri} \gamma}{(\omega_{ri}^2 + \gamma^2)^2} \frac{e^2 |\phi_1|^2}{T_e^2}. \quad (\text{VI.7})$$

The normalized values for the two terms constituting the second-order electron flux of Eq. (VI.2), $n_0 u_{\perp e2}$ and $n_0 \langle u_{\perp e1} h_{e1}^* \rangle$, have been plotted in Figure VI.1 in the case of the simulation data from [37]. From the figure it can be seen that the second order cross-field velocity is directed inwards in those regions where $\nabla_{\perp} \ln(n_0/B^2) < 0$ and outwards when the gradient changes sign, while the flux contribution due to the $n_0 \langle u_{\perp e1} h_{e1}^* \rangle$ term presents the opposite behavior. It is the competition between these two terms that will dictate whether quasi-linear transport is inward or outward in the MN.

Substituting the expressions for $\langle u_{\perp e1} h_{e1}^* \rangle$ and $u_{\perp e2}$ in Eq. (VI.2) and discarding any $O(\varepsilon)$ term,

$$(n_e u_{\perp e})_2 = n_0 c_e k^2 \rho_e^3 \omega_{LH}^2 \frac{k_{\theta} \omega_{ri} \gamma}{(\omega_{ri}^2 + \gamma^2)^2} \frac{e^2 |\phi_1|^2}{T_e^2}. \quad (\text{VI.8})$$

Eq. (VI.8) shows that the second order electron flux has the same sign of the second order velocity $\langle u_{\perp e1} h_{e1}^* \rangle$. Thus, the cross-field electron current is directed against the perpendicular gradient of n_0/B^2 . This, in practice and for radially-decreasing plasma density profiles, means that quasi-linear transport is directed away from the axis. Quasi-linear diffusion then effectively acts to quench plasma inhomogeneities. This highlights the role that instabilities have in inhomogeneous plasmas, which is that of attenuating gradient-driven drifts present at the equilibrium. Unstable oscillations, induced by the presence of said drifts, cause the plasma to migrate in a direction opposite to that of the equilibrium gradients, relaxing the inhomogeneities and therefore the induced drifts.

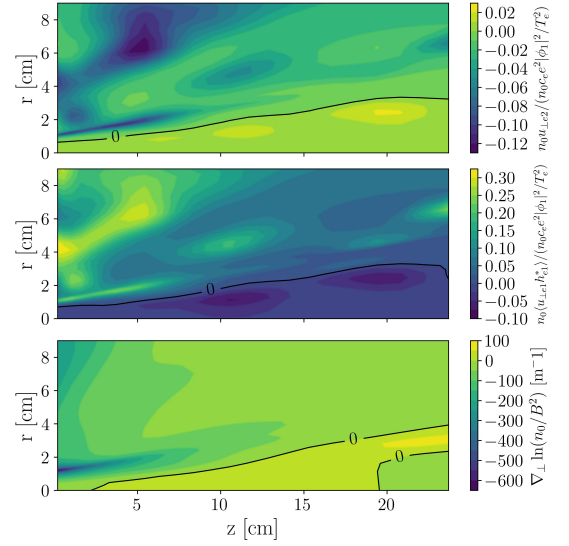


FIG. VI.1. Top: 2D map of $n_0 u_{\perp e2}$ normalized with respect to the local electron thermal flux $n_0 c_e$ and the non-dimensional wave amplitude $e^2 |\phi_1|^2 / T_e^2$. Middle: 2D map of $n_0 \langle u_{\perp e1} h_{e1}^* \rangle$ normalized with respect to the local electron thermal flux $n_0 c_e$ and the non-dimensional wave amplitude $e^2 |\phi_1|^2 / T_e^2$. Bottom: 2D map of the gradient $\nabla_{\perp} \ln(n_0/B^2)$.

VII. SUMMARY

We have derived a local linear stability model of 3D electrostatic isothermal waves in a partially magnetized plasma presenting inhomogeneities in both parallel and perpendicular directions of the magnetic field, taking into account magnetic curvature effects, parallel dynamics, gyroviscosity, collisionality, and inertial effects from a fluid perspective. The equilibrium plasma temperature has been assumed to be isotropic. The inclusion of 2D gradients of both zeroth and first-order plasma quantities represents a novelty of this work with respect to the available literature.

The presented model is based on expansions of the momentum and continuity equations in the small parameter $\varepsilon = \rho_e/L$. We have shown the detailed derivation of the dispersion relation in the Low Frequency regime, that is, $\omega_e = O(\omega_{ce} \varepsilon)$. Our proposed approach is particularly convenient for assessing the effect of plasma inhomogeneities by iteratively including larger powers of ε as shown in an earlier version of this work, presented as a conference paper in [38], detailing the application of our approach to the High Frequency regime.

From this analysis, we have provided simple and general instability criteria for both drift-gradient and drift-dissipative instabilities, highlighting the role of each drift and their interplay on the onset of drift-driven unstable oscillations and the effect of finite Larmor radius effects on the onset/quenching of exponential growth.

The dispersion relation has been specialized to the study of oscillations in the MN of a Helicon Thruster, using the data from [37] as a reference. Maps of the growth rate, real oscillation frequency and wavenumber have been provided for the most unstable modes predicted to arise in the MN, show-

ing the onset of essentially-azimuthal instabilities in the 1 kHz–1 MHz range. The analysis has highlighted the importance of including parallel inhomogeneities in the formulation of the dispersion of an $E \times B$ plasma discharge such as that of a MN, as these gradients may drive instabilities even when conditions for Modified Simon-Hoh Instability are not met and in the absence of axial propagation. Three regions of the MN can be identified: one in the upper near-plume, where perpendicular gradients are dominant, and where conditions for MSHI are respected (point A of Figure V.1); one in the lower near-plume, where conditions for MSHI are not respected, and where both perpendicular and parallel dynamics effects become important in triggering instabilities (point B); one in the far-plume, where far effects are dominant (point C). Collisional effects are shown to be secondary, at least in the explored parametric range. While based on a local, linear approximation, these findings are in qualitative agreement with some of the available experimental data, where significant spectral power density is found in this frequency range in several MNs [28, 30–32].

As a final step, we have carried out a quasi-linear analysis to gauge the second-order effect of oscillations on transport in the absence of collisions. From this study, relevant to the aforementioned low frequency regime, we have obtained the two main components of the second order electron flux, $n_0 u_{\perp e 2}$ and $n_0 \langle u_{\perp e 1} h_{e 1}^* \rangle$. The former is directed as the gradient of n_0/B^2 , while the latter is in the opposite direction; being the latter larger, $(n_e u_{\perp e})_2$ is directed against the density gradient. Then, the role of instabilities seems to be that of ‘pushing’ the plasma against the equilibrium gradients, attenuating the zeroth-order drifts which cause the plasma to destabilize in the first place. This conclusion agrees with the observations of Hepner et al. [31] of an outward electron flux, in contrast with the description from Takahashi et al. [28] of an inward

particle flux.

We stress that for this fluid model to be valid we are intrinsically limited to the study of long wavelengths, $k\rho_e < 1$, and small parallel propagation, $|c_e k_{\parallel}| < |\omega_e|$. Moreover, having assumed isothermal perturbations as a closure may not always be valid. To overcome these limitations, a more consistent as well as complex kinetic approach should be employed.

Moreover, as these instabilities grow in time, their amplitude may become comparable to the zeroth-order plasma quantities, violating the validity of the present linear stability analysis as non-linear effects become important. To understand which of these instabilities may evolve into appreciably large amplitude oscillations a more complex non-linear stability should be carried out. This, however, goes beyond the scope of this paper.

ACKNOWLEDGMENTS

This project has received funding from the European Research Council (ERC) under the European Union’s Horizon 2020 research and innovation programme (Starting Grant project ZARATHUSTRAS, grant agreement No 950466).

DATA AVAILABILITY

The simulation dataset used in this work can be accessed freely on <https://doi.org/10.5281/zenodo.10641401> under the license terms detailed therein.

Appendix A: Gyroviscous Tensor Divergence

From the definition of the gyroviscous tensor, assuming isotropic temperature $T_{\perp e} = T_{\parallel e}$ and fast-ordering dynamics [42]:

$$\begin{aligned}
 -\frac{\nabla \cdot \Pi_e}{m_e n_e} = \frac{1}{en_e} & \left[\left(\nabla \times \left(\frac{T_e n_e}{B} \mathbf{1}_{\parallel} \right) \right) \cdot \nabla \mathbf{u}_e - \frac{\nabla}{2} \left(\frac{T_e n_e}{B} \mathbf{1}_{\parallel} \cdot (\nabla \times \mathbf{u}_e) \right) \right. \\
 & + B \mathbf{1}_{\parallel} \cdot \nabla \left(\frac{T_e n_e}{B^2} \left(3 \mathbf{1}_{\parallel} \times (\mathbf{1}_{\parallel} \cdot \nabla \mathbf{u}_e) + \mathbf{1}_{\parallel} \times (\mathbf{1}_{\parallel} \times (\nabla \times \mathbf{u}_e)) + \mathbf{1}_{\parallel} \cdot \frac{\nabla \times \mathbf{u}_e}{2} \mathbf{1}_{\parallel} \right) \right) \\
 & \left. - \nabla \times \left(\frac{T_e n_e}{B} \left(\mathbf{1}_{\parallel} \cdot \nabla \mathbf{u}_e + \frac{\mathbf{1}_{\parallel}}{2} (\nabla \cdot \mathbf{u}_e - 3 \mathbf{1}_{\parallel} \cdot \nabla \mathbf{u}_e \cdot \mathbf{1}_{\parallel}) \right) \right) \right]; \quad (\text{A.1})
 \end{aligned}$$

from its expression, it is apparent that at the zeroth order $(\nabla \cdot \Pi_e / (m_e n_e))_0 = O(\omega_{ce} u_{\theta e 0} \varepsilon^2)$.

At the first order, assuming $\mathbf{u}_{e 0} \simeq u_{e \theta 0} \mathbf{1}_{\theta}$ and neglecting $O(\varepsilon^2)$ terms:

$$\begin{aligned} \left(-\frac{\nabla \cdot \Pi_e}{m_e n_e}\right)_{\perp 1} &= \frac{c_e^2}{\omega_{ce}} \left\{ \left[\frac{k_{\perp}^2 + k_{\theta}^2 + 2k_{\parallel}^2}{2} - ik_{\perp} \left(\nabla_{\perp} \ln u_{e\theta 1} + \frac{1}{2} \nabla_{\perp} \ln \left(\frac{p_{e0}}{B^2} \right) \right) - 2ik_{\parallel} \left(\nabla_{\parallel} \ln u_{e\theta 1} + \frac{1}{2} \nabla_{\parallel} \ln \left(\frac{p_{e0}}{B^3} \right) \right) \right] u_{e\theta 1} \right. \\ &\quad \left. - i \frac{ik_{\theta}}{2} \nabla_{\perp} \ln \left(\frac{p_{e0}}{B^2} \right) u_{e\perp 1} - ik_{\theta} \left[ik_{\parallel} + \nabla_{\parallel} \ln u_{e\parallel 1} + \frac{1}{2} \nabla_{\parallel} \ln \left(\frac{p_{e0}^2}{B^5} \right) \right] u_{e\parallel 1} \right\} - i \frac{c_e^2}{2\omega_{ce}} (k_{\perp} \nabla_{\perp} + 2k_{\parallel} \nabla_{\parallel}) u_{e\theta 0} \frac{p_{e1}}{p_{e0}} \quad (\text{A.2}) \end{aligned}$$

$$\begin{aligned} \left(-\frac{\nabla \cdot \Pi_e}{m_e n_e}\right)_{\theta 1} &= \frac{c_e^2}{\omega_{ce}} \left\{ - \left[\frac{k_{\perp}^2 + k_{\theta}^2 + 2k_{\parallel}^2}{2} - ik_{\perp} \left(\nabla_{\perp} \ln u_{e\perp 1} + \frac{1}{2} \nabla_{\perp} \ln \left(\frac{p_{e0}}{B^2} \right) \right) - 2ik_{\parallel} \left(\nabla_{\parallel} \ln u_{e\perp 1} + \frac{1}{2} \nabla_{\parallel} \ln \left(\frac{p_{e0}}{B} \right) \right) \right] u_{e\perp 1} \right. \\ &\quad \left. - i \frac{ik_{\theta}}{2} \nabla_{\perp} \ln \left(\frac{p_{e0}}{B^2} \right) u_{e\theta 1} + i \left[k_{\perp} \left(ik_{\parallel} + \nabla_{\parallel} \ln u_{e\parallel 1} + \frac{1}{2} \nabla_{\parallel} \ln \left(\frac{p_{e0}^2}{B^5} \right) \right) + k_{\parallel} \left(\nabla_{\perp} \ln u_{e\parallel 1} + \nabla_{\perp} \ln B \right) \right] u_{e\parallel 1} \right\} \\ &\quad + i \frac{c_e^2}{2\omega_{ce}} (k_{\theta} \nabla_{\perp} u_{e\theta 0}) \frac{p_{e1}}{p_{e0}} \quad (\text{A.3}) \end{aligned}$$

$$\begin{aligned} \left(-\frac{\nabla \cdot \Pi_e}{m_e n_e}\right)_{\parallel 1} &= \frac{ic_e^2}{\omega_{ce}} \left\{ k_{\theta} \left[ik_{\parallel} + \nabla_{\parallel} \ln u_{e\perp 1} + \frac{1}{2} \nabla_{\parallel} \ln B \right] u_{e\perp 1} - \left[k_{\perp} \left(ik_{\parallel} + \nabla_{\parallel} \ln u_{e\theta 1} + \frac{1}{2} \nabla_{\parallel} \ln B \right) \right. \right. \\ &\quad \left. \left. + k_{\parallel} \left(\nabla_{\perp} \ln u_{e\theta 1} + \nabla_{\perp} \ln \left(\frac{p_{e0}}{B^3} \right) \right) \right] u_{e\theta 1} - k_{\theta} \nabla_{\parallel} \ln \left(\frac{p_{e0}}{B^4} \right) u_{e\parallel 1} \right\} - i \frac{c_e^2}{2\omega_{ce}} (k_{\perp} \nabla_{\parallel} u_{e\theta 0}) \frac{p_{e1}}{p_{e0}}. \quad (\text{A.4}) \end{aligned}$$

At the second order, discarding any term of order $O(\varepsilon)$ with respect to $\omega_{ce} \mathbf{u}_{e2}$,

$$\begin{aligned} -\frac{\nabla \cdot \Pi_{e2}}{m_e n_0} &= \frac{c_e^2}{\omega_{ce}} \left[(\mathbf{k} \times \mathbf{1}_{\parallel}) \cdot \mathbf{k} \langle ih_{e1} (i\mathbf{u}_{e1})^* \rangle \right. \\ &\quad \left. - \frac{\mathbf{k}}{2} \langle ih_{e1} (\mathbf{1}_{\parallel} \cdot i\mathbf{k} \times \mathbf{u}_{e1})^* \rangle + \frac{\mathbf{k}}{2} \langle h_{e1} \mathbf{1}_{\parallel} \cdot \mathbf{k} \times \mathbf{u}_{e1}^* \rangle \right] = \\ &\quad \frac{c_e^2}{\omega_{ce}} \frac{\mathbf{k}}{2} \left[\mathbf{1}_{\parallel} \cdot \mathbf{k} \times \left(-\frac{ih_{e1} (-i\mathbf{u}_{e1}^*) - ih_{e1}^* i\mathbf{u}_{e1}}{4} \right. \right. \\ &\quad \left. \left. + \frac{h_{e1} \mathbf{u}_{e1}^* + h_{e1}^* \mathbf{u}_{e1}}{4} \right) \right] \exp(-2\gamma t) = 0. \quad (\text{A.5}) \end{aligned}$$

Then, $(\nabla \cdot \Pi_e / (m_e n_e))_2$ yields no contribution of order $O(\omega_{ce} \mathbf{u}_{e2})$ in the second order for of the momentum equation (VI.5).

Appendix B: Wave amplitude in presence of zeroth-order parallel gradients

The presence of gradients in our plasma imply that a wave traveling in the same direction of the gradients will experience a change in effective medium impedance as they propagate. This causes terms in the form $\nabla_{\parallel} Q_0 \nabla_{\parallel} Q_1$ to appear in the expression of the dispersion relation. If we give Q_1 an arbitrary shape, we are inadvertently introducing terms acting as artificial sources or sinks or energy. To show this, we next

discuss a wave propagating in the parallel direction, with arc length coordinate σ , described by the 1D wave equation for a generic perturbed quantity $\Psi_1(\omega, \sigma)$

$$\frac{\partial^2 \Psi_1}{\partial \sigma^2} = -k_{\sigma}^2(\omega, \sigma) \Psi_1, \quad (\text{B.1})$$

with k_{σ} real-valued function of ω and σ , and with

$$\left| \frac{\partial k_{\sigma}}{\partial \sigma} \right| \ll k_{\sigma}^2. \quad (\text{B.2})$$

We can use the WKB method to find a solution in the form of

$$\Psi_1(\omega, \sigma) \propto \exp\left(\pm i \int_{\sigma_0}^{\sigma} k_{\sigma}(\omega, s) ds\right) \quad (\text{B.3})$$

which approximately satisfies Eq. (B.1) as long as (B.2) is valid. Rewriting the same equation in a new reference frame $\zeta = \zeta(\sigma)$ yields, assuming $\zeta(\sigma)$ to be locally invertible and with $\tilde{\Psi}_1(\omega, \zeta) = \Psi_1(\omega, \sigma)$:

$$\frac{\partial^2 \tilde{\Psi}_1}{\partial \zeta^2} + \kappa(\zeta) \frac{\partial \tilde{\Psi}_1}{\partial \zeta} = - \left(\frac{\partial \zeta}{\partial \sigma} \right)^{-2} k_{\sigma}^2(\omega, \sigma(\zeta)) \tilde{\Psi}_1, \quad (\text{B.4})$$

$$\text{with } \kappa(\zeta) = \frac{\partial^2 \zeta}{\partial \sigma^2} \left(\frac{\partial \zeta}{\partial \sigma} \right)^{-2}.$$

Here, a solution in the form of $\tilde{\Psi}_1 \propto \exp(\pm i \int k'(\omega, \zeta) d\zeta)$, with k' real-valued function of ω , cannot exist, as the left-hand side of Eq. (B.4) would include a term $\pm i \kappa(\zeta) k'(\omega, \zeta)$,

while the right-hand side would still be a real-valued function of ω . Instead, applying the WKB method once again, we find a solution in the form

$$\tilde{\Psi}_1(\omega, \zeta) \propto \exp \left[\int_{\zeta_0}^{\zeta} \left(-\frac{\kappa(s)}{2} \pm ik_{\zeta}(\omega, s) \right) ds \right] \quad (\text{B.5})$$

with

$$k_{\zeta}^2(\omega, \zeta) = \left(\frac{\partial \zeta}{\partial \sigma} \right)^{-2} k_{\sigma}^2(\omega, \sigma(\zeta)) - \frac{\kappa^2(\zeta)}{4} \quad (\text{B.6})$$

a real-valued function of ω . The solution in (B.5), valid as long as the inequality in Eq. (B.2) is applicable to both κ and k_{ζ} , substituting σ with ζ , does not incur in the same problem discussed before, as both sides of Eq. (B.4) would be real-valued functions of ω . This formulation, therefore, does not induce an artificial instability onto waves in the ζ reference system.

Our dispersion relation is formally the same as that expressed in Eq. (B.4). Indeed, defining $\Phi_1 = n_0 \phi_1 B^{-1}$, the equation

$$\nabla_{\parallel}^2 [\Phi_1 \exp(ik_{\parallel} s_{\parallel})] - \nabla_{\parallel} \ln \frac{P_{e0}}{B} \nabla_{\parallel} [\Phi_1 \exp(ik_{\parallel} s_{\parallel})] = -\frac{\omega_{\parallel} + iv_e}{c_e^2} \left[\omega_{Me} - \frac{k^2 c_s^2 (\omega_{Te} + \omega_e)}{\omega_i^2 - k^2 c_s^2} \right] \Phi_1 \quad (\text{B.7})$$

corresponds to the $k\rho_e \rightarrow 0$ limit of the dispersion relation from Eq. (III.30), with the definition of Ω_{\parallel}^2 from Eq. (III.23)

and assuming the inequalities

$$|\nabla_{\parallel} k_{\parallel}| \ll k_{\parallel}^2, \quad \left| \nabla_{\parallel}^2 \ln \Phi_1 \right| \ll (\nabla_{\parallel} \ln \Phi_1)^2$$

to be valid. By applying the change of coordinates $\xi = \xi(s_{\parallel})$, with

$$\nabla_{\parallel} \ln \nabla_{\parallel} \xi = \nabla_{\parallel} \ln \frac{P_{e0}}{B}, \quad (\text{B.8})$$

we get, with $\tilde{\Phi}_1(\omega, \xi) = \Phi_1(\omega, s_{\parallel}) \exp(ik_{\parallel} s_{\parallel})$,

$$\begin{aligned} \frac{\partial^2 \tilde{\Phi}_1}{\partial \xi^2} &= -\frac{\omega_{\parallel} + iv_e}{c_e^2 (\nabla_{\parallel} \xi)^2} \left[\omega_{Me} - \frac{k^2 c_s^2 (\omega_{Te} + \omega_e)}{\omega_i^2 - k^2 c_s^2} \right] \tilde{\Phi}_1 \\ &\equiv -k_{\xi}^2(\omega, \xi) \tilde{\Phi}_1, \end{aligned} \quad (\text{B.9})$$

which is exactly the same as Eq. (B.1). Since k_{ξ}^2 is a real-valued function of ω for $v_e = 0$, it follows that k_{\parallel}^2 has to be real-valued as well, as in Eq. (B.6): subsequently, from Eq. (B.5), the shape of Φ_1 has to be

$$\nabla_{\parallel} \ln \frac{n_0 \phi_1}{B} = \frac{1}{2} \nabla_{\parallel} \ln \frac{P_{e0}}{B}, \quad (\text{B.10})$$

which is the $k\rho_e \rightarrow 0$ limit of Eq. (III.24). The same result can be reached by following the procedure shown in section III, where we imposed the imaginary part of Ω_{\parallel}^2 to be zero. The two approaches can be summarized as follows: parallel gradients don't introduce complex coefficients in the differential wave equation. Collisions, on the other hand, are energy sinks, therefore they introduce an imaginary coefficient in the dispersion relation as shown in equations (B.9) and (III.30), forcing ω to be complex [47]. A similar procedure should be applied to determine the shape of $\nabla_{\perp} \ln \phi_1$ if we were to extend the analysis to the $O(\varepsilon^2)$ order.

[1] H. Kaufman, "Technology of closed-drift thrusters," *AIAA Journal*, vol. 23, pp. 78–87, 1985.
[2] D. Goebel and I. Katz, *Fundamentals of Electric Propulsion: Ion and Hall Thrusters*. Jet Propulsion Laboratory, Pasadena, CA, 2008.
[3] E. Ahedo, "Plasmas for space propulsion," *Plasma Physics and Controlled Fusion*, vol. 53, no. 12, p. 124037, 2011.
[4] J. Navarro-Cavallé, M. Wijnen, P. Fajardo, and E. Ahedo, "Experimental characterization of a 1 kW helicon plasma thruster," *Vacuum*, vol. 149, pp. 69–73, 2018.
[5] D. Packan, P.-Q. Elias, J. Jarrige, T. Vialis, S. Correyero, S. Peterschmitt, J. Porto-Hernandez, M. Merino, A. Sánchez-Villar, E. Ahedo, G. Peyresoubes, A. Thorinius, S. Denis, K. Holste, P. Klar, S. Scharmann, J. Zorn, M. Bekemans, T. Scalais, E. Bourguignon, S. Zurbach, P. Azais, I. Habbassi, M. Mares, and A. Hoque, "H2020 MINOTOR: Magnetic nozzle electron cyclotron resonance thruster," in *36th International Electric Propulsion Conference*, no. IEPC-2019-875, (Vienna, Austria), Electric Rocket Propulsion Society, 2019.
[6] M. Merino and E. Ahedo, "Magnetic nozzles for space plasma thrusters," in *Encyclopedia of Plasma Technology* (J. L. Shohet,

ed.), vol. 2, pp. 1329–1351, Taylor and Francis, 2016.
[7] I. D. Kaganovich, A. Smolyakov, Y. Raitses, E. Ahedo, I. G. Mikellides, B. Jorns, F. Taccogna, R. Gueroult, S. Tsikata, A. Bourdon, J.-P. Boeuf, M. Keidar, A. T. Powis, M. Merino, M. Cappelli, K. Hara, J. A. Carlsson, N. J. Fisch, P. Chabert, I. Schweigert, T. Lafleur, K. Matyash, A. V. Khrabrov, R. W. Boswell, and A. Fruchtman, "Perspectives on physics of exb discharges relevant to plasma propulsion and similar technologies," *Physics of Plasmas*, vol. 27, no. 12, p. 120601, 2020.
[8] R. Hastie, J. Ramos, F. Porcelli, M. o. T. Science, and F. Center, "Drift ballooning instabilities in tokamak edge plasmas," *Physics of Plasmas*, vol. 10, no. 11, pp. 4405–4412, 2003.
[9] E. Ahedo and J. Ramos, "Parametric analysis of the two-fluid tearing instability," in *50th Annual Meeting of the APS-Division of Plasma Physics, November 2008*, 2008.
[10] J. J. Ramos, "Normal-mode-based theory of collisionless plasma waves," *Journal of Plasma Physics*, 2019.
[11] J. J. Ramos, E. Bello-Benítez, and E. Ahedo, "Local analysis of electrostatic modes in a two-fluid E x B plasma," *Physics of Plasmas*, vol. 28, no. 5, p. 052115, 2021.
[12] K. Hara, A. R. Mansour, A. C. Denig, and S. Tsikata, "Fluid

- and kinetic plasma instabilities for hall effect thrusters,” in *37th International Electric Propulsion Conference*, 2022.
- [13] J.-P. Boeuf and A. Smolyakov, “Physics and instabilities of low-temperature $E \times B$ plasmas for spacecraft propulsion and other applications,” *Physics of Plasmas*, vol. 30, no. 5, 2023.
- [14] E. Ahedo, “Using electron fluid models to analyze plasma thruster discharges,” *Journal of Electric Propulsion*, vol. 2, no. 1, p. 2, 2023.
- [15] E. Choueiri, “Plasma oscillations in Hall thrusters,” *Physics of Plasmas*, vol. 8, no. 4, pp. 1411–1426, 2001.
- [16] E. Bello-Benítez and E. Ahedo, “Advances on low-dimensionality fluid modelling of Hall thruster discharges,” in *Space Propulsion Conference 2021*, no. paper 133, (March 17–19), Association Aéronautique et Astronautique de France, 2021.
- [17] D. Poli, E. Bello-Benítez, P. Fajardo, and E. Ahedo, “Time-dependent axial fluid model of the hall thruster discharge and its plume,” *Journal of Physics D: Applied Physics*, 2023.
- [18] E. Bello-Benítez, A. Marín-Cebrián, and E. Ahedo, “Effect of injection conditions on the non-linear behavior of the ECDI and related turbulent transport,” 2024. Pre-print available at <https://arxiv.org/pdf/2405.08761>.
- [19] A. Morozov, Y. Esipchuk, A. Kapulkin, V. Nevrovskii, and V. Smirnov, “Effect of the magnetic field on a closed-electron-drift accelerator,” *Sov. Phys.-Tech. Phys.(Engl. Transl.)* 17: No. 3, 482-7 (Sep 1972)., 1972.
- [20] Y. Esipchuk and G. Tulinin, “Drift instability in a Hall-current plasma accelerator,” *Sov. Physics-Tech. Physics*, vol. 21, no. 4, pp. 417–423, 1976.
- [21] W. Frias, A. Smolyakov, I. Kaganovich, and Y. Raitses, “Long wavelength gradient drift instability in Hall plasma devices. I. Fluid theory,” *Physics of Plasmas*, vol. 19, p. 072112, 2012.
- [22] D. Escobar and E. Ahedo, “Low frequency azimuthal stability of the ionization region of the hall thruster discharge. i. local analysis,” *Physics of Plasmas*, vol. 21, no. 4, p. 043505, 2014.
- [23] A. Smolyakov, O. Chapurin, W. Frias, O. Koshkarov, I. Romadanov, T. Tang, M. Umansky, Y. Raitses, I. Kaganovich, and V. Lakhin, “Fluid theory and simulations of instabilities, turbulent transport and coherent structures in partially-magnetized plasmas of ExB discharges,” *Plasma Physics and Controlled Fusion*, vol. 59, p. 014041, 2017.
- [24] A. Litvak and N. Fisch, “Resistive instabilities in Hall current plasma discharge,” *Physics of Plasmas*, vol. 8, no. 2, pp. 648–651, 2001.
- [25] O. Buneman, “Instability of electrons drifting through ions across a magnetic field,” *Journal of Nuclear Energy. Part C, Plasma Physics, Accelerators, Thermonuclear Research*, vol. 4, no. 2, pp. 111–117, 1962.
- [26] E. Bello-Benítez and E. Ahedo, “Axial-azimuthal, high-frequency modes from global linear-stability model of a Hall thruster,” *Plasma Sources Science and Technology*, vol. 30, p. 035003, 3 2021.
- [27] N. A. Krall and P. C. Liewer, “Low-frequency instabilities in magnetic pulses,” *Physical Review A*, vol. 4, pp. 2094–2103, 1971.
- [28] K. Takahashi, C. Charles, and R. W. Boswell, “Wave-driven electron inward transport in a magnetic nozzle,” *Scientific reports*, vol. 12, no. 1, p. 20137, 2022.
- [29] D. Maddaloni, F. Boni, V. Désangles, B. Bayón-Buján, M. Merino, and F. Terragni, “Experimental characterization of oscillations in the magnetic nozzle of an electron cyclotron resonance thruster,” in *38th International Electric Propulsion Conference*, no. IEPC-2024-387, (Toulouse, France, June 23–28), Electric Rocket Propulsion Society, 2024.
- [30] D. Maddaloni, B. Bayón-Buján, J. Navarro-Cavallé, and M. Merino, “Low-frequency oscillations in the magnetic nozzle of a helicon plasma thruster,” *Plasma Sources Science and Technology (under review)*, 2024.
- [31] S. Hepner, B. Wachs, and B. Jorns, “Wave-driven non-classical electron transport in a low temperature magnetically expanding plasma,” *Applied Physics Letters*, vol. 116, no. 26, p. 263502, 2020.
- [32] A. E. Vinci, *Physics of magnetic nozzles and helicon plasma discharges*. PhD thesis, Université d’Orléans, 2022.
- [33] T. R. Desjardins and M. Gilmore, “Dynamics of flows, fluctuations, and global instability under electrode biasing in a linear plasma device,” *Physics of Plasmas*, 2016.
- [34] J. D. Huba and C. S. Wu, “Effects of a magnetic field gradient on the lower hydrid drift instability,” *The Physics of Fluids*, vol. 19, no. 7, pp. 988–994, 1976.
- [35] P. A. Sturrock, “In what sense do slow waves carry negative energy?,” *Journal of Applied Physics*, vol. 31, no. 11, 1960.
- [36] A. Hasegawa, *Plasma Instabilities and Nonlinear Effects*. Springer-Verlag, 1975.
- [37] P. Jiménez, J. Zhou, J. Navarro-Cavallé, P. Fajardo, M. Merino, and E. Ahedo, “Analysis of a cusped helicon plasma thruster discharge,” *Plasma Sources Science and Technology*, vol. 32, no. 10, p. 105013, 2023.
- [38] M. Ripoli, M. Merino, and E. Ahedo, “Analysis of drift instabilities in magnetic nozzles,” in *38th International Electric Propulsion Conference*, no. IEPC-2024-506, (Toulouse, France, June 23–28), Electric Rocket Propulsion Society, 2024.
- [39] S. Andersen, V. Jensen, P. Nielsen, and N. D’Angelo, “Continuous supersonic plasma wind tunnel,” *Phys. Fluids*, vol. 12, no. 3, pp. 557–560, 1969.
- [40] E. Ahedo and M. Merino, “Two-dimensional supersonic plasma acceleration in a magnetic nozzle,” *Physics of Plasmas*, vol. 17, no. 7, p. 073501, 2010.
- [41] J. Zhou, G. Sánchez-Arriaga, and E. Ahedo, “Time-dependent expansion of a weakly-collisional plasma beam in a paraxial magnetic nozzle,” *Plasma Sources Science and Technology*, vol. 30, no. 4, p. 045009, 2021.
- [42] J. Ramos, “General expression of the gyroviscous force,” *Physics of Plasmas*, vol. 12, no. 11, p. 112301, 2005.
- [43] J. Vranjes and S. Poedts, “The universally growing mode in the solar atmosphere: coronal heating by drift waves,” *Monthly Notices of the Royal Astronomical Society*, 2009.
- [44] R. Z. Sagdeev, A. A. Galeev, T. M. O’Neil, and D. L. Book, “Nonlinear plasma theory,” 1969.
- [45] J. Zhou, A. Domínguez-Vázquez, P. Fajardo, and E. Ahedo, “Magnetized fluid electron model within a two-dimensional hybrid simulation code for electrodeless plasma thrusters,” *Plasma Sources Science and Technology*, vol. 31, no. 4, p. 045021, 2022.
- [46] J. Perales-Díaz, A. Domínguez-Vázquez, P. Fajardo, E. Ahedo, F. Faraji, M. Reza, and T. Andreussi, “Hybrid plasma simulations of the HT5k thruster,” in *ExB Plasmas Workshop, Young researchers "poster" mini-session*, (Madrid, Spain, February 16–18), 2022.
- [47] T. H. Stix, *Waves in plasmas*. Springer Science & Business Media, 1992.